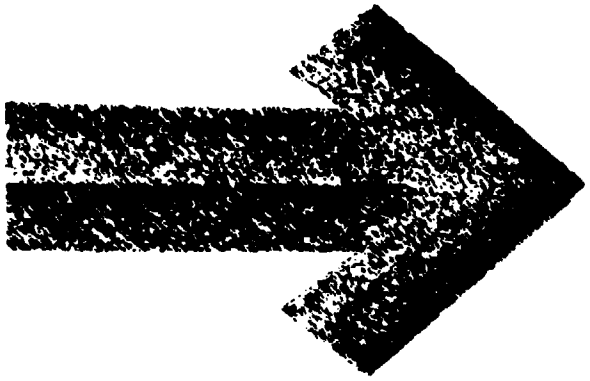

NP-12642
*Report Number*



**United States Atomic Energy Commission**
***Division of Technical Information***

OTI-131(May 1962)

USAEC Division of Technical Information Extension, Oak Ridge, Tennessee

# AN INVESTIGATION OF THE LOW EXCITED STATES OF $Cr^{52}$

by

Robert Roland Wilson

B.S., United States Naval Academy, 1952

A Thesis submitted to the Faculty of the Graduate School of the University of Colorado in partial fulfillment of the requirements for the Degree Master of Science
Department of Physics
1961

This Thesis for the M.S. degree by

Robert Roland Wilson

has been approved for the

Department of

Physics

by.

_____

_____

Date _____

## ABSTRACT


Wilson, Robert Roland (M.S., Physics)
An Investigation of the Low Excited States of $Cr^{52}$.
Thesis directed by Associate Professor Jack J. Kraushaar.

The low excited state of $Cr^{52}$ [illegible] investigated by studying the decay of $Mn^{52}$ with 3 NaI(Tl) crystals (1 large, 2 small) as singles and in coincidence gating a 200-channel pulse height analyzer. The results of a concurrent study of $Mn^{52}$ decay with the University of Colorado $\sqrt{2}$ double-focusing beta-ray spectrometer are also presented. The energies given are those of the beta-ray spectrometer studies, and the intensities given are those of the weighted average of the results of both spectrometers. The gamma-ray energies and intensities reported were (all Kev): 1433.6 ± 0.4 (100%), 1332 ± 1 (5.8%), 1245.6 ± 0.4 (6.2%), 1214 ± 1 (2.8%), 935.1 ± 0.4 (87.1%), 847.4 ± 0.6 (2.3%), 743.8 ± 0.3 (84.0%), 345.74 ± 0.08 (0.9%), annihilation quanta (65.5%). Weak transitions seen were: 2650 ± 30 (0.08%), 1463 ± 2 (0.3%), 1180 ± 20 (1.4%), 1070 ± 20 (3.2%), 630 ± 60 (2.4%).

New decay schemes for $Mn^{52}$ and $Mn^{52m}$ were proposed. The energy, spin, and parity of the excited levels of $Cr^{52}$ were given as (all Mev): 3.832 (5+,6+), 3.800 (2+), 3.74 (7±), 3.614 (5+,6+), 3.480 (3+), 3.161 (1-,2-,3-), 3.112 (6+), 2.965 (2+, 3+), 2.766 (4+), 2.648 (0+), 2.369 (4+), and 1.434 (2+).

Of interest is the 5 newly proposed excited levels of highest energy, the 9 newly reported gamma rays, the intensity differences of the 3 main transition gamma rays from those previously reported, the support given to the assignment of spin and parity by D. M. Van Patter to the triplet between 3.112 and 2.369 Mev, and the assignment to the 3.161 Mev level as the first odd parity state.


This abstract of about 250 words is approved as to form and content. I recommend its publication.

Signed _____

Instructor in charge of dissertation

* [illegible] of 2 Pi.

## ACKNOWLEDGEMENTS

It is a pleasure for the author to be able to express his gratitude to Prof. J. J. Kraushaar for suggesting the problem discussed in this paper, and for his continued support and guidance throughout the experiment.

To Prof. A. A. Bartlett, designer and builder of the beta-ray spectrometer, and Robert A. Ristinen, his co-worker, the entire credit is due for the precise energy values listed herein, and the author takes this opportunity to thank them both for their long hours of data taking.

Roger H. Berger assisted throughout the investigation by taking data, reducing this data by tedious means, and maintaining the scintillation spectrometer. Without his help the job could not have been done on schedule and the author is very grateful for his cheerful assistance.

The author is also indebted to the Atomic Energy Commission for the financial support for this research, to the Physics Department which furnished much equipment, and to the Nuclear Physics Laboratory Staff for the technical assistance given.




## TABLE OF CONTENTS


| | Page |
|---|---|
| List of Figures | |
| List of Tables | |
| Chapter 1. | |
| Introduction. | 1 |
| Chapter 2. | |
| A History of the $Cr^{52}$ Isotope. | 4 |
| Chapter 3. | |
| Experimental Method. | |
| 3.1. Scintillation Spectroscopy. | 13 |
| 3.2. Source Preparation. | 15 |
| 3.3. Multichannel Pulse Height Analyzer. | 16 |
| 3.4. Singles Method. | 18 |
| 3.5. Variables in Scintillation Spectroscopy. | 21 |
| 3.6. Coincidence Method. | 22 |
| Chapter 4. | |
| Technique of Data Analysis and Error Analysis. | |
| 4.1. Singles Analysis. | 32 |
| 4.2. Coincidence Analysis. | 36 |
| 4.3. Error Analysis. | 38 |
| Chapter 5. | |
| Experimental Results and Level Scheme Assignment. | |
| 5.1. Single Crystal Gamma-Ray Spectrometer. | 40 |
| 5.2. Double Crystal Coincidence Spectrometer | 42 |
| 5.3. Revised Decay Scheme of $Mn^{52}$. | 45 |
| 5.4. Comparison of Results of this Paper. | 48 |
| 5.5. Log ft Values for the Revised Decay Scheme. | 50 |

# MASTER COPY RECORD-SUPPLEMENTAL SHEET

REPORT NUMBER: NP-12663

## COPY DISTRIBUTION

| NO COPIES | INST. CODE | AUTH. BY | DATE | NO. COPIES | INST. CODE | AUTH. BY | DATE | NO. COPIES | INST. CODE | AUTH. BY | DATE | NO. COPIES | INST. CODE | AUTH. BY | DATE |
|---|---|---|---|---|---|---|---|---|---|---|---|---|---|---|---|
| | ACB | | | | DUP | | | | MLM | | | | SANL | | |
| | ACC | | | | DUPA | | | | NAA | | | | SAP | | |
| | AECE | | | | EBR | | | | NACA | | | | SCAO | | |
| | AECW | | | | EGGN | | | | NACW | | | | SEP | | |
| | AGC | | | | GCI | | | | NBL | | | | SFA | | |
| | AGN | | | | GDA | | | | NBS | | | | SFOO | | |
| | ANL | | | | CECE | | | | NDA | | | | SLE | | |
| | ARPA | | | | GLMM | | | | NED | | | | SPA | | |
| | AS | | | | GOO | | | | NEPA | | | | TCB | | |
| | BABS | | | | HOO | | | | NLC | | | | TSPA | | |
| | BABV | | | | HW | | | | NMEC | | | | UCLA | | |
| | BBCB | | | | IOO | | | | NRL | | | | UCI | | |
| | BMI | | | | IOOO | | | | NYOO | | | | UCRL | | |
| | BNL | | | | ISC | | | | NYUC | | | | TIOA B | | |
| | BOE | | | | JPL | | | | OMC | | | | WAPD | | |
| | BPB | | | | K-25 | | | | ORNL | | | | WARD | | |
| | BPBA | | | | KAPL | | | | ORO | | | | WAT | | |
| | CEND | | | | LA | | | | OSG | | | | WECC | | |
| | CERD | | | | LAOV | | | | OTAC | | | | WPGY | | |
| | CONB | | | | LOMS | | | | PADC | | | | WPSI | | |
| | COO | | | | MCWH | | | | PITR | | | | Y-12 | | |
| | CRM | | | | METC | | | | PPR | | | | | | |
| | CVNP | | | | MHI | | | | PRDC | | | | | | |
| | DCD | | | | MITB | | | | RWC | | | | | | |
| | DRI | | | | MITK | | | | SAND | | | | | | |



## SUBSEQUENT AND SPECIAL DISTRIBUTION

| PRINTED COPY DISTRIBUTION | | | | MICROCARDS | | PRINTED COPY DISTRIBUTION | | | | MICROCARDS | |
|---|---|---|---|---|---|---|---|---|---|---|---|
| NO COPIES | INSTALLATION AND/OR CODE | AUTH. BY | DATE | NO. SETS | DATE DIST. | NO. COPIES | INSTALLATION AND/OR CODE | AUTH. BY | DATE | NO. SETS | DATE DIST |
| | | | | | | | | | | | |
| | | | | | | | | | | | |
| | | | | | | | | | | | |
| | | | | | | | | | | | |
| | | | | | | | | | | | |
| | | | | | | | | | | | |
| | | | | | | | | | | | |
| | | | | | | | | | | | |
| | | | | | | | | | | | |
| | | | | | | | | | | | |

### DELETED COPY DISTRIBUTION

| NO COPIES | INSTALLATION CODE | AUTH. BY | DATE | DIST. BY | DATE |
|---|---|---|---|---|---|
| | | | | | |
| | | | | | |
| | | | | | |

DELETE AS FOLLOWS:

① _____

② _____

③ _____

I certify that deletions, as specified by the numbered paragraph above, were made and that these deletions were destroyed by burning.

① Name _____ Title _____ Date _____ Copy No. _____

② Name _____ Title _____ Date _____ Copy No. _____

③ Name _____ Title _____ Date _____ Copy No. _____

NR

# AN INVESTIGATION OF THE LOW EXCITED STATES OF $Cr^{52}$

by

Robert Roland Wilson

B.S., United States Naval Academy, 1952

A Thesis submitted to the Faculty of the Graduate School of the University of Colorado in partial fulfillment of the requirements for the Degree

Master of Science

Department of Physics

1961

Page

Chapter 6.

Discussion of Results.

6.1. Branching Ratios of $Mn^{52}$ Decay. 53

6.2. The Results of Hausman et al. Compared to Those of Mazari et al. 55

6.3. The Results of Katoh et al. and $Mn^{52m}$. 58

6.4. Proposed Decay Scheme of $Mn^{52m}$. 59

6.5. $V^{52} \rightarrow Cr^{52}$ Beta Decay. 60

6.6. Theoretical Points of Interest. 61

Appendix A.

Construction of Intrinsic Efficiency Curves for NaI(Tl) Crystals. A-1

Appendix B.

Variation in Shape of a Gamma Ray as a Function of Analyzer Gain or Channel Number. B-1

Appendix C.

Variation in Shape of a Gamma Ray when it is the Sum of Two Other Gamma Rays. C-1

Appendix D.

Calibration Procedure for the Model 302 Universal Coincidence Circuit. D-1

Figures 1 through 16.

LIST OF TABLES

Page

I. History of $Cr^{52}$. 5

II. Particle Reactions of $Cr^{52}$. 10

III. Sample Data for the Calculation of Relative Intensities for (3-3/4" x 3") NaI(Tl) Crystal at 14 cm. 35

IV. Intensities of Gamma Rays in Large Crystal Singles, and Intensities of Gamma Rays Coincident with the 0.935-and 0.744 Mev Gamma Rays. 41

V. Intensities of Gamma Rays Coincident with the 1.43 Mev Gamma Ray. 43

VI. Gamma Ray Intensities in Decay of $Mn^{52}$. 47

VII. Energy Levels of $Cr^{52}$. 48

VIII. Comparison of Energy Values of the Main Transition Gamma Rays of $Cr^{52}$. 49

IX. Log ft Values for $Mn^{52} \rightarrow Cr^{52}$. 51

X. Branching Ratios of $Mn^{52} \rightarrow Cr^{52}$. 53

XI. Energy Levels of $Cr^{52}$ from Hausman et al. 56

XII. Calculation of Levels Given by Mazari et al. 57

XIII. Log ft Values for $Mn^{52m} \rightarrow Cr^{52}$. 59

A-I. Photoelectric peak area/total area. A-1

A-II. Relative intensities of selected gamma rays. A-4

A-III. Relative intrinsic efficiencies of known gamma rays for a (3-3/4" x 3") NaI(Tl) crystal. A-4

A-IV. Relative intrinsic efficiencies of known gamma rays for a (2" x 2") NaI(Tl) crystal. A-5

## List of Figures


1. Decay Scheme of $Mn^{52}$ as Previously Reported.
2. $Mn^{52}$ Gamma-Ray Spectrum Singles.
3. Singles Geometry and Circuit.
4. Fast-Slow Coincidence Circuit.
5. $Mn^{52}$ Gamma-Ray Spectrum Coincident with the 1.43 Mev Gamma Ray.
6. $Mn^{52}$ Gamma-Ray Spectrum Coincident with the 1.33 Mev Gamma Ray.
7. Fast Coincidence Circuit.
8. $Mn^{52}$ Gamma-Ray Spectrum Coincident with the 0.935 Mev Gamma Ray.
9. $Mn^{52}$ Gamma-Ray Spectrum Coincident with the 0.744 Mev Gamma Ray.
10. Revised Decay Scheme of $Mn^{52}$.
11. Intrinsic Efficiency of a (3-3/4" x 3") NaI(Tl) Crystal.
12. Intrinsic Efficiency of a (2" x 2") NaI(Tl) Crystal.
13. Variation of Gamma-Ray Shape as a Function of Channel Number.
14. Sum-Peak Shape Versus a Normal Gamma-Ray Shape.
15. Model 302 Universal Coincidence Discriminator Calibration Curve.
16. Proposed Decay Scheme for $Mn^{52m}$.


## CHAPTER 1

## INTRODUCTION

One of the broad classes into which nuclei have been divided for ease of systematic analysis is that of even-even nuclei. An area which has not received a great deal of attention is the $40 \leq A \leq 92$ region, and contained therein is the interesting group of nuclei with $40 \leq A \leq 56$ which have particles outside of a closed shell in the $f_{7/2}$ state. This particular area has been the subject of calculations by Lawson and Uretsky,[1] by Raz,[2] by Kelly and Moszkowski,[3] by Shakin and Kermin,[4] and by Kisslinger and Sorensen.[5] Necessary adjuncts to any such calculations are appropriate experimental data to compare with these theories.

The present experiment on $Cr^{52}$ is a continuation of the study of nuclei in the $f_{7/2}$'s region which was commenced at the University of Colorado by a study of the $Ca^{42}$ and $Ca^{44}$ isotopes. $Cr^{52}$ has 24 protons and a closed shell of 28 neutrons with the 4 protons which are outside of the closed shell being in the $f_{7/2}$'s state.

The experiment was conducted by observing the decay of $Mn^{52}$ with two scintillation gamma-ray spectrometers in coincidence gating a 200 channel pulse-height analyzer. A concurrent study of $Mn^{52}$ was conducted by another group at the University of Colorado using a $\sqrt{2}$ π double-focusing beta-ray spectrometer. The energies of the more prominent transitions reported here were measured by internal and external conversion in the beta-ray spectrometer. These latter results were consistent with those of the scintillation studies.

A revised decay scheme was constructed with the addition of three new upper levels at 3.614 Mev with a spin of 5 or 6, 3.74 and 3.832 Mev the spin of which is uncertain. Nine new gamma rays are being reported in addition to the three main transitions and annihilation quanta gamma ray previously reported.

From an analysis of the intensities of these gamma rays the EC/$\beta^+$ ratio was recalculated to be 1.50 instead of approximately 2 as has been consistently reported heretofore. Apparent reasons for this anomaly are also discussed.

This investigation was made during a 9 month period commencing in August of 1960. There were 411 separate runs of all types made on the gamma-ray scintillation spectrometer in support of this research. Of the runs which were analyzed for gamma ray content and for their respective intensities, 10 were made on the large single crystal spectrometer and 29 were made on the double crystal coincidence spectrometer. 19 of the 29 were of the spectrum of those gamma rays in coincidence with the 1.43 Mev gamma ray. 5 of the 29 were of the 0.935 Mev coincidence spectrum, and the remaining 5 were of the 0.744 Mev spectrum.

In Chapter 2 the history of $Cr^{52}$ is discussed briefly, and the experimental method used to obtain the above results is given in Chapter 3. The technique used to analyze the data obtained in the scintillation studies is presented in Chapter 4, while the compilation of the results and the construction of the revised decay scheme is given in Chapter 5. Chapter 6 contains a discussion of the implications of this new decay scheme in the theory of even-even nuclei with emphasis on the $f_{7/2}$ nucleon region.



## References for Chapter 1


1. R. D. Lawson, and J. L. Uretsky, Phys. Rev., 106, 1369 (1957).

2. B. J. Raz, Bull. Am. Phys. Soc., 3, 224 (1958) and Phys. Rev. 114, 1116 (1959).

3. P. S. Kelley and S. A. Moszkowski, Z. Physik, 158, 304 (1960).

4. C. Shakin and A. K. Kerman, Private communication.

5. L. S. Kisslinger and R. A. Sorensen, Kgl. Danske Videnskab. Selskab, Mat.-fys. Medd., 32, no. 9 (1960).

## CHAPTER 2
## A History of the $Cr^{52}$ Isotope

There are a number of ways in which a history such as this could be presented. Since this chapter is meant only to give a survey of the increase in knowledge of the isotope it was thought that a chronological table would be the most appropriate form in that all of the facts could be assimilated at a glance. Table I outlines this history. Some literature concerning even-even nuclei is also listed as a matter of interest. Table II lists reaction studies which give the energy of the first excited state of $Cr^{52}$.

Fig. 1 displays the decay scheme of $Mn^{52}$ as of April 1961. Of particular interest is the firm establishment of the ground state of $Mn^{52}$ as $6^+$,[p,y,z] and the primary decay sequence being $6^+(\beta^+)$ $6^+(\gamma)$ $4^+(\gamma)$ $2^+(\gamma)$ $0^+$. The energy levels are those reported by Mazari et al[l] except for the one at 3.109 Mev which was assigned by Konijn et al.[r] The spin assignments to the triplet states between the 3.109 and 2.369 Mev levels as well as the possible spins of th 3.161 Mev level were assigned by Van Patter.[bb] This decay scheme does not reflect the results of Katoh et al[w] who reported new levels and transitions in December 1960 since there was a delay in receipt of their Japanese journal. The results of Katoh et al will be discussed in detail in Chapter 6.

TABLE I. History of $Cr^{52}$

| Date | Investigators | Methods | Remarks |
|---|---|---|---|
| 1946 | Peacock and Deutsch[a] | Decay of $Mn^{52}$ | Found Fermi plot was straight and thus decay was simple to 3.13 Mev level. Made first decay scheme of 3.13-, 2.40-, 1.46 Mev levels, and reported 0.510 ± 0.01, 0.734 ± 0.015, 0.940 ± 0.02, and 1.46 ± 0.03 gamma rays all Mev, 35% positron. |
| 1946 | Good, Peaslee, and Deutsch[b] | Decay of $Mn^{52}$ | Reported $\beta^+/EC + \beta^+ = (0.35 \pm 0.02)$, and $EC/\beta^+ = (1.86 \pm 0.17)$. |
| 1950 | Way et al[c] | Tabulation | Refers to above papers. |
| 1951 | Goldhaber and Sunyar[d] | Theory/Tabulation | First pointed out that the first excited state of even-even nuclei usually has spin and parity of 2+. |
| 1952 | Hausman et al[e] | 8 Mev (p,p') | Reported levels at 1.46-, 2.43-, and 3.01 Mev. |

(cont'd)

TABLE I (cont'd)

| Date | Investigators | Methods | Remarks |
|---|---|---|---|
| 1957 | Mazari et al[l] | 6.5 Mev (p,p') | Assigned all energies to levels of Fig. 1 except that of 3.109 Mev. Suggests $Mn^{52}$ decays to 3.161 Mev level in $Cr^{52}$. Said (2.368 → 0) transition was less than 6% of 1.43 Mev γ ray. |
| 1957 | Abraham et al[m] | Paramag. Res. | Assigns I = 6 or 7 to $Mn^{52}$. |
| 1957 | Lawson and Uretsky[n] | Theory | Predict 1.43 Mev level to be (2+), and calculate it to be 1.41 Mev. |
| 1958 | El Bedewi and Tadros[o] | 8.7 Mev (d,d') Angular distribution | Assigned (2+) to 1.44 ± 0.02 Mev level. |
| 1958 | Ambler et al[p] | β+ Angular correlation | Assign (6+) to ground state of $Mn^{52}$. Say (7+) is ruled out. |
| 1958 | Strominger et al[q] | Tabulation | Assigns $Mn^{52}$ decay to 3.161 Mev level of $Cr^{52}$. |

(cont'd)

TABLE I (cont'd)

| Date | Investigators | Methods | Remarks |
|---|---|---|---|
| 1958 | Konijn et al[r] | Decay of $Mn^{52}$ | EC/β+ = 1.99 ± 0.06. Say 3.109 Mev level involved in $Mn^{52}$ decay and not 3.161 Mev. EC/β + = 2.03 ± 0.06 is theoretical value. |
| 1958 | Porter et al[s] | 4.3-4.6 Mev (p, p') | 1.432 ± 0.005 Mev seen, but not 2.368 ± 0.004 Mev of Mazari. |
| 1958 | Raz[t] | Theory | Added 2 $f_{7/2}$ particles to Bohr-Mottelson model. |
| 1959 | Van Patter[u] | Tabulation | E2 transition of (2'+ → 2+) and (2'+ → 0+). |
| 1959 | Mandeville et al[v] | 1.5-5.0 Mev (p, p') | Systematic study of low levels of even-even nuclei. |
| 1959 | Ofer and Schwarzchild[w] | Nucl. Res. | Lifetime of (2+) in $Cr^{52}$ is (0.8 ± 0.2 m|sec.) |
| 1960 | Kelly and Moszkowski[x] | Theory | Constructed j-j coupled wave-functions using a central average potential perturbed by 4 $f_{7/2}$ holes. |

(cont'd)

∞

TABLE I (cont'd)

| Date | Investigators | Methods | Remarks |
|---|---|---|---|
| 1960 | Katoh et al[y] | Decay of $Mn^{52}$, and $\gamma_1 \gamma_2 \gamma_3$ angular correlation | Report $\gamma$ rays of 746.8 ± .02, 938.1 ± 0.4, and 1434.7 ± 0.8 Kev all at equal intensity. Report weak $\gamma$'s at 1.33 and 1.2 Mev at 5% and 3% of 1.43 Mev resp. Corroborate spin and parities of 6+, 4+, 2+. In decay of $Mn^{52m}$ report 1.52 (2%), 1.37, 1.15 (2%), 1.02 (3%), 0.94 (4%), 0.70 (3%) coin. with 1.43 Mev $\gamma$ ray. |
| 1960 | Kedzie | Paramag. Res. | Assigns I = 6 to $Mn^{52}$. |
| 1960 | Shakin and Kermin[aa] | Theory | Added a cubic term to harmonic oscillator description of nuclear vibrations. |
| 1961 | Van Patter[bb] | 3.3 Mev (n, n' $\gamma$) | Assigned spins and parities of 2.65 (0+), 2.77 ($\geq$ 4), 2.96 (2+), and 3.16 (1, 2, or 3) all Mev. |

TABLE I (cont'd)

| Date | Investigators | Methods | Remarks |
|---|---|---|---|
| 1960 | Katoh et al[y] | Decay of $Mn^{52}$, and $\gamma_1\ \gamma_2\ \gamma_3$ angular correlation | Report $\gamma$ rays of 746.8 ± .02, 938.1 ± 0.4, and 1434.7 ± 0.8 Kev all at equal intensity. Report weak $\gamma$'s at 1.33 and 1.2 Mev at 5% and 3% of 1.43 Mev resp. Corroborate spin and parities of 6+, 4+, 2+. In decay of $Mn^{52m}$ report 1.52 (2%), 1.37, 1.15 (2%), 1.02 (3%), 0.94 (4%), 0.70 (3%) coin. with 1.43 Mev $\gamma$ ray. |
| 1960 | Kedzie | Paramag. Res. | Assigns I = 6 to $Mn^{52}$. |
| 1960 | Shakin and Kermin[aa] | Theory | Added a cubic term to harmonic oscillator description of nuclear vibrations. |
| 1961 | Van Patter[bb] | 3.3 Mev (n, n' $\gamma$) | Assigned spins and parities of 2.65 (0+), 2.77 ($\geq$ 4), 2.96 (2+), and 3.16 (1, 2, or 3) all Mev. |

TABLE II. Reaction Studies on $Cr^{52}$ Yielding the Energy of the First Excited State.

| Date | Reaction | Mev. | Investigator |
|---|---|---|---|
| 1952 | 8 Mev (p,p') | 1.45 ± 0.02 | Hausman et al[e] |
| 1956 | (n,n') | 1.44 ± 0.05 | Beghian et al[cc] |
| 1957 | 4.4 Mev (n,n') | 1.455 ± 0.10 | Sinclair[dd] |
| 1957 | 6.51 Mev $Mn^{55}$ (p,α) | 1.434 ± 0.016 | Mazari et al[l] |
| 1957 | 6.51 Mev (p,p') | 1.433 ± 0.005 | Mazari et al[l] |
| 1958 | 4.4 Mev (p,p') | 1.432 ± 0.005 | Porter et al[s] |
| 1958 | 8.7 Mev (d,d') | 1.44 ± 0.02 | El Bedewi and Tadros[o] |
| 1957 | Theoretical | 1.41 | Lawson and Uretsky[n] |



## References for Tables I and II


a. W. C. Peacock, and M. Deutsch, Phys. Rev. 69, 306 (1946).

b. W. M. Good, D. Peaslee, and M. Deutsch, Phys. Rev. 69, 313 (1946).

c. K Way, L. Fano, M. Scott, and K. Thew, Nuclear Data, (NBS 499, 1950) p. 47.

d. M. Goldhaber and A. Sunyar, Phys. Rev. 83, 906 (1951).

e. H. J. Hausman, A. J. Allen, J. S. Arthur, R. S. Bender, and C. J. McDole, Phys. Rev., 88, 1296 (1952).

f. M. J. Glaubman, Phys. Rev., 90, 1000 (1953).

g. R. Sehr, Z. Physik, 137, 523 (1954).

h. K. Way, R. W. King, C. L. McGinnis, R. van Lieshout, Nuclear Level Schemes, AEC TID-5300, GPO, 1955.

i. G. Scharff-Goldhaber and J. Weneser, Phys. Rev., 98, 212 (1955).

j. G. M. Temmer and N. P. Heydenburg, Phys. Rev. 99, 1609 (1955).

k. W. J. Huiskamp, M. J. Steenland, A. R. Miedema, H. A. Tolhoek, and C. J. Gorter, Physica, 22, 587 (1956).

l. M. Mazari, W. W. Buechner, and A. Sperduto, Phys. Rev., 107, 1383 (1957).

m. M. Abraham, C. D. Jeffries, R. W. Kedzie, and O. S. Leifson, Bull. Am. Phys. Soc., Ser II, 2, 382 (1957).

n. R. D. Lawson, and J. L. Uretsky, Phys. Rev., 106, 1369 (1957).

o. F. A. El Bedewi and S. Tadros, Nuclear Phys., 6, 434 (1958).

p. E. Ambler, R. W. Hayward, D. D. Hoppes, and R. P. Hudson, Phys. Rev., 110, 787 (1958).

q. D. Strominger, J. M. Hollander, and G. T. Seaborg, Rev. Mod. Phys., 30, 2, II (1958).

r. J. Konijn, B. Van Nooijn, and H. L. Hagedoorn, Physica, 24, 377 (1958).

s. W. C. Porter, D. M. Van Patter, M. A. Rothman, and C. E. Mandeville, Phys. Rev. 112, 467 (1958).

t. B. J. Raz, Bull. Am. Phys. Soc. 3, 224 (1958).

u. D. M. Van Patter, Nuclear Phys., 14, 42 (1959).

v. C. E. Mandeville, D. M. Van Patter, W. C. Porter, M. A. Rothman, and C. P. Swann, AFOSR-TR-59-28, 1959.

w. S. Ofer and A. Schwarzchild, Phys. Rev. Lett., 3, 384 (1959).

x. P. S. Kelley and S. A. Moszkowski, Z. Physik, 158, 304 (1960).

y. T. Katoh, M. Nozawa, Y. Yoshizawa, and Y. Koh, J. Phys. Soc. Japan, 15, 2140 (1960).

z. R. W. Kedzie, Phys. Rev., 117, 1056 (1960).

aa. C. Shakin and A. K. Kerman. Private communication.

bb. D. M. Van Patter, Bull. Am. Phys. Soc., 6, (1961).

cc. L. E. Beghian, D. Hicks, and B. Milman, Phil. Mag. 1, 261 (1956).

dd. R. M. Sinclair, Phys. Rev., 107, 1306 (1957).



# CHAPTER 3

# EXPERIMENTAL METHOD

## 3.1 Scintillation Spectroscopy

Before commencing the description of the scintillation apparatus in particular, it may be helpful to discuss scintillation spectroscopy in general. There are several recent theories[1,2] extant relative to the mechanism which produces the photons in the crystal as opposed to the general description of an "ionizing action" which is a little vague. A quantitative discussion of the mechanism would be out of place here but it is hoped that a brief qualitative discussion would prove to be interesting.

There appears to be two model mechanisms which are major candidates for the excitation process: electron-hole pairs and excitons. Other effects were considered[2] but their contribution seemed to be minor in comparison to these two.

Sodium iodide being an ionic crystalline semiconductor has exciton bands, as well as a conduction band, and a periodic potential structure in Block's treatment. Excitons can be created and valence band electrons can be raised to the conduction band by Coulomb excitation from collision processes of the primary electrons which occur from gamma-ray photoelectric effect, Compton scattering, and pair production. The thallium ions, having a concentration of 0.1% in our crystals,[3] have a greater ionization potential than do the sodium ions which they replace and thus perform as attractive centers for any diffusing excited electrons. One of the differences between electron-hole pairs and the exciton model is that the two are bound together in the exciton whereas they

are not in the pairs. Thus, a conduction electron can be captured by a thallium ion converting it to a ground state thallium atom. This atom can then capture a hole creating a thallium ion in an excited state and its subsequent de-excitation by a dipole transition creates the photons. The arrival of an exciton at the thallium activity center causes the same action except that the electron and hole arrive more or less simultaneously. Dekker[4] gives the lifetime of an exciton as $10^{-8}$ seconds with a diffusion speed of $10^{7}$ cm/sec. (the speed of thermal electrons) and a resulting mean free path of $10^{-4}$ cm.

Van Sciver[5] shows that the fluorescence of sodium iodide with thallium is much more pronounced at -190°C (liquid nitrogen) than at 20°C. A possible explanation being that at 20°C there is a slight lattice rearrangement near the activity site as a result of the presence of the excited ion creating a pronounced possibility of a non-radiative transition[6,7] to the ground state. At -190°C this lattice rearrangement is retarded and the non-radiative transitions are greatly reduced necessitating the de-excitation process to be mainly radiative.

The scintillation counter consists of three parts: a crystal phosphor, a photomultiplier tube, and the associated electronic circuitry. 1944 saw the first successful coupling of a scintillation phosphor to a photomultiplier tube to detect radiations. The rapid growth of this type of counter lies in the development of all three components. This interest centers mainly on scintillation phosphors as opposed to other types of detectors because of their:

a. high sensitivity to gamma rays,
b. wide range of physical size,
c. response being proportional to the incident radiation, and



d. fast decay times.

Scintillation spectrometers have an advantage over beta-ray spectrometers in that very low activity sources can be used for successful analysis. Sodium iodide crystals are hygroscopic and therefore are hermetically sealed.

3.2 Source Preparation

The supplier of the $Mn^{52}$ was the Nuclear Science and Engineering Corporation in Pittsburgh and the sources were produced by the (Cr + p) reaction. Chromium powder was irradiated and dissolved in H Cl. The resulting solution, containing iron carrier, is poured carefully into a mixture of NaOH and $Br_2$. The chromium is oxidized to soluble chromate, while the manganese is oxidized to $MnO_2$ and co-precipitates with $Fe(OH)_3$. The $Fe(OH)_3$ is filtered off and dissolved in H Cl. The entire process is repeated, then the iron is removed by an ion exchanger, leaving carrier-free $Mn^{52}$ in the eluate. This eluate is evaporated to dryness and the residue is dissolved in about 0.5 N HCl. The radio-chemical purity was greater than 98%. The first source was received near the first of August 1960, the second on December 22, 1960 (30 mr/hr at 12"), and the third on March 10, 1961 (90 mr/hr at 12"). Because of the chemical form, the sources required no special preparation or separation and they were usable upon receipt.

To standardize our procedure and reduce the number of variables as much as possible we investigated the energies of the beta particles of our manganese source, as well as those of all of the sources we intended to use for calibration, in order to calculate the optimum thickness of the bottom of a lucite singles bottle and the side of a lucite coincidence bottle. We desired to have the container thick

enough to stop nearly all beta particles but not so thick as to absorb too much energy of any weak gamma rays. Using the range-energy relationship for electrons of Katz and Penfold[8] it was determined that one-tenth of an inch of lucite for our windows would be sufficient. We proceeded to manufacture identical lucite source cups for our calibration sources and for the $Mn^{52}$ source.

3.3 Multi-channel Pulse Height Analyzer

When a gamma ray of a given energy is converted inside of a scintillation crystal it can be completely absorbed by a photoelectric event or by creation of an electron-positron pair, or it can be partially absorbed by undergoing a Compton scattering event. Thus, the output of an associated photomultiplier tube can be a continuously varying series of pulses starting with a very small pulse denoting a small Compton event and ending at a large pulse denoting complete absorption of the gamma ray by a photoelectric event.

The RIDL* 200 channel pulse height analyzer sorts this continuous series of pulses by size. For every input pulse accepted for analysis, the analog-to-digital converter generates a train of constant amplitude output pulses, the number of the pulses in this train being directly proportional to the amplitude of the input pulse. This pulse train is then processed by a digital computer, so that if the number of pulses in the train is N, one count will be stored in the memory at channel N.

The elapsed time for this counting operation is given by $(20 + 0.5N)\mu$ seconds and is called the "dead" time of the analyzer since the input channel to the analog-to-digital

* Radiation Instrument Development Laboratory, Chicago, Ill.



converter is closed to incoming pulses until after the counting and storage operation has been completed. This dead time is indicated on a meter on the front of the analyzer and is given as percent of the analyzer's capacity to perform these operations.

Strong sources, or sources which are placed too close to the scintillation crystal, provide enough counts per second to almost fully occupy the capacity of the analyzer to perform. It was found that to have no distortion in the cathode-ray tube display it was necessary that the dead time be kept at 30% or below.

Conversely, the length of time that the analyzer is capable of receiving pulses is the "live" time. Experimental runs are measured in "live" time as opposed to "elapsed" time since elapsed time would include the time the analyzer is computing and this cannot be used for absolute source activity measurements. This is because computing time is a function of pulse height whereas activity is not. Thus, when activities are compared, as for example the half-lives of isotopes, the live time of the analyzer is required in order to obviate each run having to be corrected for dead time later. In the Model 34-2 this is done automatically.

The gain of the amplifier in the analyzer is the control by which the operator selects the voltage reference for calibration purposes. The cathode-ray tube displays one illuminated image point for each channel and these are numbered horizontally and consecutively. The height of each point from zero reflects the number of counts put in that channel. Thus, for the photo-peak, the statistical distribution of the size of the incoming pulses yields a normal distribution curve, and for a single gamma ray one sees such a curve on the

cathode-ray tube. The energy corresponding to the channel at which the apex of this distribution curve is found is designated as the energy of the gamma ray (pulse distribution) which caused it.

The gamma-ray spectrometer is calibrated by using radioactive sources the energies of the gamma rays of which have been accurately measured such as $Zn^{65}$, $Na^{22}$, $Cs^{137}$, $Co^{60}$, $Pr^{144}$, or ThC''($Tl^{208}$). The position of these known gamma-ray pulse distributions on the cathode-ray tube determines the "energy to channel number" relation used. Changing the analyzer gain moves the distribution to the left or right on the cathode-ray tube setting in a new energy to channel correspondence. A plot of the energy of the gamma rays of such sources versus the channel number position of each gamma ray yields a calibration curve such as seen in Fig. 15 of Appendix D.

A gamma-ray scintillation spectrum is a superposition of many such distributions and for a complex nuclei of, say, 10 gamma rays it is the purpose of analysis (Chapter 4) to separate this conglomeration into an ordered, quantitative determination of the intensities and energies of all components.

### 3.4 Singles Method

The initial step in the analysis was to get an overall look at the gamma-ray spectrum and to attempt to arrive at some preliminary intensity figures. Fig. 2 is such a study which had a 1000 minute live time. To accomplish this we used a large single NaI(Tl) scintillation crystal in a circuit which drove the 200-channel pulse-height analyzer as shown in Fig. 3. We used a 3-3/4" x 3" crystal, factory mounted, to a 5075EX phototube of 5" diameter. Although 3" phototubes were available (Dumont 6363 for example) an increase in



efficiency is realized by using larger phototubes to reduce edge effects.[9] The resolution of a crystal-photomultiplier combination is given by

$$\frac{\Delta E_{\frac{1}{2}}}{E} = \text{resolution}, \qquad (3.1)$$

where $\Delta E_{\frac{1}{2}}$ is the width of the peak at half maximum and E is the peak energy, we found the resolution of the (3-3/4" x 3") crystal to be 12% using $Cs^{137}$ although the factory packing slip stated the resolution to be 9.1%.

There was the usual background due to cosmic rays and stray radiation and we reduced this by encasing the crystal in a lead house with 2" walls and 2-3/4" top. There was a 7/8" hole in the roof over a tapered collimating opening in which we placed the source cup and since the source was outside of the hole backscattering was eliminated.

In addition to the source cup thickness we standardized the geometry further by having the bottom surface of the source cup, which was in contact with the liquid, lie in the plane of the top of the lead cover as shown in Fig. 3. All sources would then be 14 cm from the top of the large singles crystal. We considered this 14 cm position to be the "standard" or "normal" geometry and a source to crystal distance of 30 cm. to be the "high" geometry. It is necessary to have "set" geometries in order to have continuity throughout the investigation. Referring to equation A.1 of Appendix A the probability of a count in the photo-peak is $N_p = \varepsilon P \Omega N_o$ for a given gamma ray. The probability of a sum peak is then the product:

$$N_s = (\varepsilon P \Omega N_o)_1 (\varepsilon P \Omega N_o)_2$$
$$= (\varepsilon P N_o)_1 (\varepsilon P N_o)_2 \Omega^2 \qquad (3.2)$$

The relative intensity then of a sum peak to a real gamma ray

is then of the order of Ω. When the source to crystal distance is doubled this relative intensity is decreased by a factor of 1/4. Thus, by doubling the distance from the source to the crystal relative contributions of real and sum gamma rays are easily seen as illustrated in Fig. 2.

It was mentioned above that the background was reduced by enclosing the crystal in a lead house. It was not eliminated, however, and the thorium in the lead bricks contributed its undesired spectrum along with other active elements. We ran a background for most runs just after, or before, a scheduled run thereby insuring a good match in analyzer calibration so that by subtracting the background from the run only the desired spectrum remained.

Two difficulties were noticeable and only one of which was controllable. These presumably were saturation of the photo-cathode and/or space charge effect of the photo-tube and drift. Saturation and/or space charge effects are noticeable as non-linearity of the analyzer during calibration.[10] This was prevented by keeping the source strength limited to the point of having the 200-channel analyzer dead time be always under 30%. It appeared that 40% dead time was near the non-linearity threshold.

Part of the drift problem was reduced by the replacement of a locally constructed, and rather old, high voltage supply by a highly stabilized (0-2999) volt one manufactured by the Fluke Company. This replacement not only allowed very long runs for the singles but also for the coincidence circuit since we used this supply for the coincidence phototubes also. This replacement did not eliminate other circuit caused drifts.



## 3.5 Variables in Scintillation Spectroscopy

In gamma-ray scintillation spectroscopy there are many variables which affect the spectrum presentation on the cathode-ray tube of the pulse-height analyzer which is in turn a visual display of the data in the memory of the analyzer. These variables are:

a. Variation of gamma-ray photo efficiency in the scintillation crystal with gamma-ray energy.
b. Variation in shape of a gamma ray of a given energy with gain setting or channel of the pulse-height analyzer (PHA).
c. Variation in shape of a gamma ray when this gamma ray is the sum of two other gamma rays.
d. Variation in shape of a gamma ray of a given energy with variation in source to crystal distance.

In practice, the last variation listed had relatively little effect compared to the magnitudes of the other three.

The first type of variation depends on the material of which the scintillation crystal is made, the size and shape of the crystal, and the energy of the gamma ray. The fourth type of variation is normally included with this one but operationally it is easier to consider them as separate functions and treat this first variation by using a fixed source to crystal distance.

Appendix A considers this first type of function, Appendix B considers the second type, while Appendix C considers the third type.

In practice, the first type of variation is reduced to a graph called an "Intrinsic Efficiency Curve" (See Figs. 11 and 12, Appendix A). The use of these intrinsic efficiency curves is discussed in Chapter 4. It is unfortunate that

reliable curves of this type are not catalogued for various sized sodium iodide crystals and various source to crystal distances. Heath's catalogue[11] lists curves but our large crystal was not covered and the smaller crystals used in the coincidence circuit were difficult to interpolate. Miller and Snow[12] have made a detailed study of this effect by using a Monte Carlo calculation. Unfortunately they considered cylindrical crystals whose height was twice the width. Our crystals had roughly the same height as width. Since the absorption is not linear, interpolation was impossible. Therefore, one could not compare their calculated results to our experimental results. We did compare Heath's experimental results to ours for the (2" x 2") crystal with fair agreement as seen in Appendix A, Fig. 12.

The experimental procedure for obtaining the data for Appendix A was to put the largest gamma ray of standard calibration sources near channel 150 of the 200 channel PHA. This channel setting gave better statistics for the gamma-ray shape. We then analyzed these plotted results to obtain the relative intensities of the gamma rays present. (See Appendix A for details). The relative intensities were already known from published data. We then compared these intensities and obtained ratios for the intrinsic efficiencies of 2 gamma rays. By assuming a value for the intrinsic efficiency of one gamma ray this ratio determined the value for the other gamma ray. A plot of these for all known gamma rays used should yield a smooth curve. The values assumed were adjusted until the best fit was obtained. The results are seen in Fig. 11 and Fig. 12 of Appendix A.

3.6 Coincidence Method

From the results of the single crystal method we should



have a complete spectrum of all of the gamma rays emitted by the nucleus. But, in order to construct a unified decay scheme it is necessary to obtain an ordering of the separate gamma rays. Of the various modes of decay available from the mother to the daughter nucleus, and of the various modes of de-excitation in cascade available in the daughter nucleus, only one mode for each occurs for any given decaying nucleus. By measuring as many of these modes as possible we can consolidate these results and determine the relative probability for any one of them and thus arrive at a decay scheme.

The experimental method of achieving this is the fast-slow coincidence method. In this method we use two crystal counters instead of one as shown in Fig. 4. We require that one selected gamma ray enters counter #1 which is a (1-3/4" x 2") NaI(Tl) crystal, while all of the others associated with it are counted in detector #2 which is a (2" x 2") NaI(Tl) crystal. In order to differentiate between all of the various modes, the time available for the counting of the associated gamma rays entering detector #2 is limited by a fast coincidence circuit.

There is always the possibility that gamma rays from two separate nuclei arrive at the counters at the same time and are counted. These are referred to as "chance" coincidences and will be discussed later.

Briefly the process is as follows. In the #1 circuit there is a single channel pulse-height analyzer (Model 302 Universal Coincidence Circuit) the discriminator of which is set to pass only those pulse heights corresponding to our selected gamma ray. Pulses from counter #2 are amplified and then delayed by 3μ secs before going to the PHA to compensate for the delay by the rest of the circuitry of the gate pulse.

When a gamma ray is absorbed in each crystal at the same time, then a pulse from each counter arrives at the fast coincidence circuit at nearly the same time. These pulses have a finite width and the fast coincidence circuit is designed to transmit a signal only if the two pulses arrive within the resolving time ($2\tau$) of the circuit. If such a signal is transmitted, then, after amplification, it enters side #2 of the slow coincidence circuit. If the gamma ray which entered crystal #1 is of the energy which was pre-set on the discriminator of the slow coincidence circuit, then its pulse combines with the fast coincidence signal to send a slow coincidence pulse to the 200 channel analyzer as a gating pulse. This allows the analyzer to record only the energies of those gamma rays which are in coincidence (same decay mode or cascade mode) with the preselected gamma ray.

It was mentioned that the timing pulse used was taken directly from the anode of the photomultiplier. For these time measurements only the first few electrons of a pulse are used.[13] The reason for this is that the decay time of the sodium iodide is $2.5 \times 10^{-7}$ seconds[14] while the resolution of our coincidence circuit is $\sim 10^{-8}$ seconds and all of the electrons can not be counted before a coincidence is measured. In addition, we only use the information that an event occurred and the leading edge of the pulse contains this. The rise times of the Hewlett-Packard 460AR wide band amplifiers in our circuit were rated at $3 \times 10^{-9}$ seconds and each had a delay time of $14 \times 10^{-9}$ seconds thus insuring excellent response.

The pulses do not arrive at the fast coincidence circuit at precisely the same time since there are statistical variations because of the crystal decay time and because



of delays incurred also in the phototube.

RCA 6810A photomultiplier tubes were used in the two coincidence counters and the (2" x 2") crystal had a resolution of 9% using $Cs^{137}$. This is one of the fastest tubes available[15] except for pre-production design prototypes, and for energy determination (in circuit #2) there is only one other tube listed[15] as having a slight edge in performance. Thus, this tube offered the optimum of those available.

Fig. 7 displays the fast coincidence circuit of Wenzel[16] A Rossi-type diode coincidencecircuit is preceded by a limiter tube (Amperex E180F) in each channel to reduce pulse height sensitivity of this type of circuit as described in Wenzel's report.[16] The limiter tubes, normally conducting, are used to keep the coincidence circuit independent of the incoming pulse. All diodes are the G7A type, since these are among the fastest in response. The $D_1$ diodes are provided a bias which is adjusted so that each diode draws little current, about 1 ma, and is easily turned off. The negative input pulse is limited, the positive pulse is clipped in the plate circuit by the delay line preceding the diode, and then it turns off $D_1$. The other diode then carries all of the current of both so that the voltage on the plate line remains nearly constant. If both diodes are turned off, the plate voltage rises to B+ and a positive pulse is sent through the pulse-stretching diode $D_2$ to a slow amplifier which acts also as a discriminator. Its grid is biased so that the single diode $D_1$ cut-off pulse is not passed but the larger pulse from a double cut-off is amplified.

There are many ways to determine the resolving time of such a circuit. This time amounts to twice the length of

time that one diode $D_1$ can be turned off, which is determined by the rise time of the pulse from the limiter tube and the amount of clipping used. Two pulses entering the two sides within this time are considered to be coincident. Of course, this can happen by chance wherein the two gamma rays are not in real coincidence at all. We employ precisely this idea to help determine the resolving time.

First, consider using only one source of gamma rays. Attach the output of one crystal-phototube combination to both inputs of the coincidence circuit and have its output, in turn, sent to a counter after appropriate amplification. The output will then be exactly coincident. Now put a variable delay line in one of the two input lines. As this delay is increased the number of counts stored per unit time decreases. If a plot is made of counts per unit time versus delay time, a gaussian peak results with the apex at zero delay time.[17] The resolving time is defined as the full width at half the maximum number of counts. Since the delay time is $\tau$ and measured from the abscissa point under the maximum, the resolving time is then $2\tau$.

Now, if a given source registers $N_1$ counts per second, then there will be $(2\tau N_1)$ of these counts stored within the time $2\tau$. This, then, is the probability of these counts occurring. If we take two separate sources, then the probability of their occurring at the same time is a product: $(2\tau N_1)(2\tau N_2)$. By definition we can say that the number of chance coincidences occurring within $2\tau$ is then $(2\tau N_{ch})$ which is equal to the above product, or:

$$N_{ch} = 2\tau N_1 N_2 \qquad (3.2)$$

One method we used to determine $2\tau$ was to use two different sources, $Na^{22}$ and $Cs^{137}$, placed so that a lead shielding



between them exposed only one of them to one counter. Any coincidence counts observed with this geometry should be chances. By counting each separately we then got $N_1$ and $N_2$. Thus, $2\tau$ was determined using equation (3.2). The result was $2\tau = 3.6 \times 10^{-8}$ seconds.

As another check we used $Co^{60}$ and put a delay line of 215 m$\mu$ seconds in one side to get chance counts and used one side of the circuit to register $N_1$, and the other side to get $N_2$. The result was $2\tau = 5.0 \times 10^{-8}$ seconds.

The relatively long half life of 5.7 days for $Mn^{52}$ did not require special procedures[18] to determine chances since the longest run made was only 3-1/2 days, and we assumed that the chance rate remained constant during the runs.

From equation (3.2) we see that $N_{ch}$ is a function of the source strength squared since both $N_1$ and $N_2$ are each a function of the source strength. We thus must use as small a source strength as we can, yet enough to get good statistics. In practice, we found by making actual runs to get chances that, as long as we satisfied the 30% dead time requirement discussed earlier, the chances were negligible for the runs under consideration.

The method of selecting the discriminator voltage settings on the slow coincidence circuit is discussed in Appendix D. This is critical for if the voltage window is too large then those gamma rays with energies in the vicinity of the desired one can also trigger the gate, and you then record the radiations in coincidence with them as well as those in coincidence with the desired one. As seen in the 1.43 Mev coincidence spectrum of Fig. 5, the 1.24 Mev and the 1.33 Mev gamma rays are very close to the 1.43 Mev line. For a considerable time we used a window which was too wide, giving us results which were impossible to resolve. When the window was narrowed down

to the point of selecting only small portions of the photo-peak, rather than all of it, we then began getting excellent results.

We used an amplifier in the #1 counter circuit to increase the pulse height for the #1 discriminator. We found that the 6810A photomultiplier gave such a strong pulse out of the pre-amplifier that this pulse over-loaded the amplifier and gave us non-linear results. An attenuator placed in the line after the pre-amplifier corrected this. Incidentally, it is this high performance of the 6810A which allows us to take the pulse from the anode directly for the input to the wide band amplifiers.

In addition to gamma rays whose photo-peaks are in the near vicinity of the selected gamma ray contributing to the triggering, the Compton effect of real gamma rays with energy larger than the selected one also yield pulses which can trigger the system. Fig. 8 and Fig. 9 are of the 0.935 Mev and 0.744 Mev gamma-ray coincidence spectra, respectively, and they illustrate what a large contribution this Compton triggering can make. We selected a window size and positioned it to obtain the 0.935 Mev spectrum. We knew that the Compton pulses of the 1.43 Mev, 1.33 Mev, and 1.24 Mev gamma rays were all triggering the circuit allowing the 0.935 Mev gamma ray to enter counter #2 and be counted. The magnitude of this effect is seen by the presence of the 0.935 Mev gamma in its own spectrum. We positioned the window used just to the right of the 0.935 Mev gamma ray so that only these Compton pulses would trigger the circuit. We ran this second run under the same conditions of time, geometry, source strength, etc., so that a superposition plot could be made. This plot is indicated in Fig. 8. Its subtraction then should



yield a close approximation to the true spectrum. In Chapter 4 this is discussed in more detail.

This same effect is realized by the larger sum peaks of two real gamma rays triggering the circuit. We found, however, that this contributes a negligible amount.

## References for Chapter 3


1. A. J. Dekker, Solid State Physics, (Prentice-Hall Inc. Englewood Cliffs, N. J. 1957) p. 399.
2. Nuclear Electronics (International Atomic Energy Agency, Austria, 1959) p. 37.
3. Scintillation Phosphors, (Harshaw Chemical Co., Cleveland, 1960) p. 24.
4. Dekker, op. cit., pp. 374 and 401.
5. Nuclear Electronics, op. cit., p. 38.
6. S. C. Curran, Luminescence and the Scintillation Counter, (Academic Press, Inc., London, 1953), p. 77.
7. Dekker, op. cit., p. 401.
8. F. Ajzenberg-Selove, Nuclear Spectroscopy, (Academic Press, New York, 1960), Part A, p. 29.
9. DuMont Multiplier Photo Tubes, (A. B. DuMont Laboratories, Inc., New Jersey, 1959) 2nd. ed., p. 15.
10. Ibid. p. 16.
11. R. L. Heath, Scintillation Spectroscopy Gamma-Ray Spectrum Catalogue, (Phillips Petroleum Co., 1957) IDO-16408.
12. W. F. Miller and W. J. Snow, Monte Carlo Calculation of the Energy Loss Spectra for Gamma-Rays in Sodium Iodide and Cesium Iodide, (Argonne National Laboratory, 1961) ANL-6318.
13. Ajzenberg-Selove, op. cit., p. 34.
14. Scintillation Phosphors, op. cit., p. 10.
15. Nuclear Electronics, op. cit., p. 4.





16. W. A. Wenzel, (University of California Radiation Laboratory Report, UCRL 8000, 1957).
17. Nuclear Electronics, op. cit., p. 9.
18. K. Siegbahn, Beta-and Gamma-Ray Spectroscopy, (Interscience Publishers, Inc., New York, 1955), p. 205.

# CHAPTER 4

## Technique of Data Analysis and Error Analysis

### 4.1 Singles Analysis

The spectrum of any radioactive isotope as displayed on the cathode-ray tube of a multichannel pulse height analyzer is a locus of points the heights of which are dependent upon the number of counts stored in the memory of each channel. For complex nuclei each of the several gamma rays emitted has a total pulse height distribution (gamma-ray shape) dependent upon its energy, and this distribution is composed of photoelectric events, Compton events, and electron-positron pairs as discussed in Chapter 3 and Appendix B. Every channel then contains pulses of each type from many different gamma rays. In order to separate the total counts in each channel so as to determine quantitatively how many of the counts are the result of each of the different gamma rays a subtraction process is used.

A calibration curve is made using known calibration sources. The isotope to be analyzed is used as a source for a run and the results of this run are plotted. (See Fig. 2 as an example.) Using the calibration curve the energies corresponding to the channel numbers of the obvious gamma rays on this plot are read off and assigned tentatively to each of the unknown gamma rays. An unknown gamma ray in the spectrum which is prominent, and has relatively the highest energy, such as the 1.43 Mev gamma ray, is selected as the starting point for this subtraction process. For the present we will ignor any complicating effects such as sum peaks. Having chosen the 1.43 Mev gamma ray we must now take a known source which has a single gamma ray of this energy and, using



the analyzer, make a run such that this single gamma ray is at the same channel as the 1.43 Mev gamma ray. We do this in order to obtain the shape of a gamma ray having this energy using this particular equipment.

In practice, this is impossible since such convenient isotopes are non-existent. It is necessary to use isotopes with gamma rays which are near the energy desired and also be rather prominent. To be most precise, it is best to get a larger and a smaller energy gamma ray to set at the chosen channel. A super position plot of one on the other such that their apexes match will allow an interpolation to be made using the three energies of 2 known calibration sources and the 1 known subject source. (For example, see the dashed curve gamma-ray shape in Fig. 13).

In the particular case of $Mn^{52}$ we used $K^{42}$ with its 1.53 Mev gamma ray as a subtraction gamma ray for the 1.43 Mev gamma ray. The 1.28 gamma ray of $Na^{22}$ was used for the 1.24 and 1.33 Mev gamma rays. $Zn^{65}$ having a 1.114 Mev gamma ray was used for the 0.935 Mev gamma ray. $Mn^{54}$ has a 0.842 Mev gamma ray which could be used both for the 0.935 Mev and the 0.744 Mev gamma rays. The 0.511 Mev gamma ray of $Na^{22}$ worked nicely for the annihilation quanta of $Mn^{52}$.

Having obtained the requisite subtraction curves the first step is to match the leading (right side) edge and the apexes of the gamma ray of $K^{42}$ to that of the 1.43 Mev gamma ray of $Mn^{52}$. The matching of the apexes and leading edge is the result of a basic assumption that all of the counts in these channels are due solely to a real gamma ray at that intensity and we wish to take all of it out. Later we will see that after this is done and the entire subtraction process is completed this original assumption is changed and various

contributions are used to arrive at a more realistic intensity. The entire shape of the $K^{42}$ curve is traced on the original drawing of $Mn^{52}$. The value of each point of the $K^{42}$ curve is subtracted, channel by channel, from the value of the point on the $Mn^{52}$ curve yielding a difference curve. (See Fig. 5 for details, since that drawing is very illustrative). The leading edge of the next prominent gamma ray that appears is of the 1.33 Mev gamma. Using the appropriate energy related curve we use the same technique obtaining a second difference curve with the 1.24 Mev gamma ray now the prominent gamma ray to be taken out. In this fashion, the totality of points in any one channel is distributed among various gamma rays according to what contribution each apparently made to this total.

The shape of the gamma ray used for subtraction is therefore a very critical matter since the presence of low intensity gamma rays can be lost if due regard is not given. This subtlety is seen in the shape of the points defining the 1.06 and 0.63 Mev gamma rays in Fig. 6. Using this method gamma rays of the order of 1% of the intensity of the 1.43 Mev gamma ray were clearly identified.

The relative intensities are computed by using equation A.3 of Appendix A. Table III below illustrates such a computation.



TABLE III. Sample data for the calculation of relative intensities for 3-3β4" x 3" NaI(Tl) crystal at 14 cm.

| γ-Ray Energy | Peak Height (Counts) | Half Widths | Intrinsic Efficiency | Product | Relative Intensity to 1.43 Mev |
|---|---|---|---|---|---|
| 1.43 | $1.85 \times 10^6$ | 3.77 | .43 | $1.62 \times 10^7$ | 100% |
| 0.935 | $3.1 \times 10^6$ | 2.36 | .54 | $1.36 \times 10^7$ | 83.9% |
| 0.744 | $3.9 \times 10^6$ | 2.25 | .62 | $1.41 \times 10^7$ | 87.7% |

One complication to this process is the occurrence of a sum peak at or near the channel at which a gamma ray to be taken out is positioned. The problem is to determine how much of the heights of these points are due to the sum peak and how much are due to the real gamma ray. As mentioned earlier a change in source to crystal distance will reduce the sum peak contribution. An alternate method which is applicable in some cases is to find another sum peak on the original drawing. (See Appendix D for the shape of a sum peak). After the entire analysis has been finished, multiply the product of the derived areas (h $W_{\frac{1}{2}}$ experimental) of each of the gamma rays contributing to this sum by a constant, K, and set this total product equal to the area (h $W_{\frac{1}{2}}$ experimental) of the sum peak. This computation derives from the probability of 2 events occurring at the same time. It is the product of their individual probabilities. This constant, K, thus determined can, in turn be used to calculate the area (h $W_{\frac{1}{2}}$) of the desired sum peak. The appropriate $W_{\frac{1}{2}}$ for this sum peak is approximately the square root of the sum of the squares of the half widths of the two real gamma rays involved. In general, this method is not satisfactory if the constant,

$K_s$ is derived for sum peaks not appearing on the original drawing. A study was initiated in the course of this experiment to obtain a relationship between this sum peak constant and the crystal-geometry combination employed but no definitive results were realized.

4.2 Coincidence Analysis

It was mentioned in Chapter 3 that the gating discriminator can be triggered by Compton event pulses of real gamma rays which are larger than the one selected as reference or these pulses can be the result of two real gamma rays entering the crystal at the same time causing a sum peak distribution. Fig. 8 shows the contribution of this effect plotted as a dashed line. The technique used to obtain this curve was discussed in Chapter 3. The contribution to the 1.43 Mev gamma ray in this Figure is clearly seen. This entire curve is subtracted from the original data to yield the first difference curve as shown by the solid circles. It is seen that the entire 0.935 Mev gamma ray has been removed since ideally it should not appear in its own coincidence spectrum. The process is now the same from here on for this run as for the singles technique described in paragraph 4.1.

This technique has the advantage that it firmly establishes the contribution to the complete curve by the Compton contributions. A detailed analysis should yield the gamma rays in coincidence with the 0.935 Mev gamma ray in their true intensities. A possible drawback is that this bulk subtraction may cause some weak gamma rays to be missed since this is an approximation. In Fig. 8 the 0.847 Mev gamma ray can be seen as the difference between the solid circles and the Compton of the 1.43 Mev subtraction curve.



But, the approximation fails sometimes since a little to the right of channel 120 one obtains negative numbers if one were to be literal with the technique.

In the absence of a convenient flat Compton expanse on the high side of the selected gamma ray on which to set the discriminator, as in the case of the 0.935 Mev gamma ray, one must try to construct such a total Compton contribution. Fig. 9 displays the 0.744 Mev coincidence spectrum in which this very situation exists. The dashed curve is one which was constructed. The original data curve is the result of the true 0.744 Mev coincidence spectrum as well as the coincidence spectra of the 0.935, 1.24, 1.33, and 1.43 Mev gamma rays in proportion to their intensities in the 0.744 Mev region near channels 80 - 90. It was necessary to construct a coincidence spectrum for each of these gamma rays unless one already was available. This was necessary only in the case of the 1.24 Mev gamma ray. Figs. 5, 6, and 8 were the curves available for the others.

To construct the 1.24 Mev coincidence spectrum it, too, was the result of higher energy Compton triggering by the 1.33 and 1.43 Mev gamma rays. From an estimated decay scheme sequence based on data already derived, it was assumed what a pure 1.24 Mev spectrum would look like. Compton contributions were judiciously added by adding the 1.33 and 1.43 Mev coincidence spectra.

These four spectra of 0.935, 1.24, 1.33, and 1.43 Mev gamma rays were now combined to yield an estimated Compton contribution. The dashed curve of Fig. 9 is the result. Subtracting it from the original data yielded the solid circle curve which in turn was analyzed in detail. It can be seen how the 0.744 Mev gamma ray was removed from its coincidence run by this process.

## 4.3 Error Analysis

It is impossible to assign quantitative errors to any intensities derived by this technique which are based on quantitative systematics of the apparatus since the bulk of the error is qualitative in origin. The intrinsic efficiency curves themselves have errors in them which stem from the effects to be discussed presently. But, for any given energy, the scale on the intrinsic efficiency curve ordinate is expanded enough so that the error resulting from a small vertical displacement of the curves is under 2%. The basis for this figure results from a calculation of the relative intensity of the 0.935 Mev gamma ray to that of the 1.43 Mev gamma ray using both the 14 cm and 30 cm curves. The difference was only 4%. An estimated deviation of the 14 cm line could be at most one-half of this.

The major contributions to the error of this technique are listed below:

a. Having an imperfect knowledge of the shape of subtraction gamma rays, and not having such a curve for each specific energy required for a specific isotope;

b. The multiple subtraction process which generates cumulative errors at each subtraction since the scale on the log paper is of a size such that only the first three significant figures can be used regardless of the magnitude of the number of counts in a channel (For instance, a small change of 500 counts is a significant contribution but when it is subtracted from a 65,000 count peak the difference is barely discernable. Thus, low energy gamma rays, i.e. 0.70 Mev and under in $Mn^{52}$, of low intensities are not reported with much positiveness. However, the higher the energy of a gamma ray the fewer subtractions were required to obtain it and hence its intenaity is more certain.);



c. The Compton triggering of the gating circuit, as discussed previously, generates manifold problems which are impossible or at best extremely difficult to surmount and then they are only partially allayed;

d. Drifts were experienced but the magnitude was slight. (In the present experiment the longest run made was of the 1.33 Mev coincidence which had a 5000 minute live time duration. The total drift was 5 channels all of which occurred in the last 1000 minutes and the spectrum was easily corrected by re-adding the last 1000 minutes at the proper channels. Fig. 6 demonstrates that long runs can yield excellent results. In fact, it was this run which allowed the scintillation spectroscopy group to display the 0.346 Mev gamma ray which was not possible in any of the other runs. The beta-ray spectrometer group found this gamma ray early in their experiment.);

e. The error in reading the energy from the calibration curve is estimated at ± 0.01 Mev and this is based upon an error of ± 1 channel in reading the gamma ray position from the plot ( The gross variations in the energies assigned to gamma rays in the figures result from the gross errors discussed in a., b., and c. above and not from the misreading of the calibration curve or its inherent errors.)

In summary, the errors assigned to the gamma ray intensities as found in these scintillation studies were the result of using a simple arithmetic average and taking the root-mean-square deviation as the error.

# CHAPTER 5

## Experimental Results and Level Scheme Assignment

### 5.1 Single Crystal Gamma-Ray Spectrometer

The single crystal studies performed at the beginning of the experiment allowed us to get an overall view of the $Mn^{52}$ decay spectrum. Fig. 2 presents the typical singles spectrum and this particular run had a live time of 1000 minutes. Because of the complexity of this spectrum only 2 of the gamma rays of second or third order magnitude intensity relative to the 1.43 Mev gamma ray are shown, i.e. 1.24 and 1.33 Mev. The change in height of the gamma rays between channels 100 and 160 as the source to crystal distance is changed indicates that these are sum peaks. It also indicates that no real gamma rays exist in this area of any appreciable magnitude.

The sum peaks for 1.24 + 1.43 Mev and 1.33 + 1.43 Mev gamma rays were calculated and are shown as 2.67 and 2.76 Mev respectively. Their sum has been subtracted from the original data and it appears that a real gamma ray may exist of 2.65 Mev energy with a relative intensity of 0.08% of the 1.43 Mev gamma ray.

Table IV presents the results of the large single crystal runs and the errors assigned are rms although the uncertainty is actually of the order of 10%. The important result shown there is that the intensities of the 0.935 and 0.744 Mev gamma rays are not the same as that of the 1.43 Mev gamma ray as has been consistently reported in the literature prior to this experiment.

TABLE IV. Intensities of Gamma Rays in Large Crystal Singles and Intensities of Gamma Rays Coincident with the 0.935- and 0.744 Mev Gamma Rays.

| γ-Ray | Large Singles | | | | 0.935 Mev Coincidence | | | 0.744 Mev Coincidence | | |
|---|---|---|---|---|---|---|---|---|---|---|
| Mev | #A | #40 | #53 | Ave. | #267 | #104 | Ave. | #273 | #107 | Ave. |
| 1.43 | 100 | 100 | 100 | 100 | Present | Present | Present | Present | Present | Present |
| 1.33 | - | - | - | - | - | - | - | - | - | - |
| 1.24 | - | - | - | - | 5.4 | 7.4 | 6.4 ± 1.0 | - | - | - |
| 1.18 | - | - | - | - | - | - | - | - | - | - |
| 1.07 | - | - | - | - | - | 1.4 | 1.3 ± 1.0 | - | - | - |
| 0.93 | 82.3 | 83.9 | 78.3 | 81.5 ± 4.0 | 88.4[a] | 82.5[a] | 85.4 ± 3.1 | Present | Present | Present |
| 0.84 | - | - | - | - | 3.8 | 3.9 | 3.9 ± 1.0 | - | - | - |
| 0.74 | 79.8 | 87.7 | 82.1 | 83.2 ± 5.8 | 84.0[b] | 84.0[b] | 84.0[b] | - | - | - |
| 0.63 | - | - | - | - | 1.5 | 3.9 | 2.7 ± 1.2 | 3.8 | 4.3 | 4.1 ± 0.3 |
| 0.51 | 59.7 | 72.3 | 58.9 | 63.6 ± 6.1 | 61.0 | 62.7 | 71.8 ± 0.9 | 67.0 | 64.7 | 65.* ± 1.2 |
| Min. Live Time | 1000 | 1000 | 1000 | - | 2000 | 1500 | - | 1000 | 1000 | - |

a. From intensity of .743 Mev γ-Ray.

b. Used for normalization.

## 5.2 Double Crystal Coincidence Spectrometer

The value of the coincidence method lies in its ability to eliminate background, to separate cascade sequences and thus to relatively intensify real gamma rays, and to help determine cascade sequences. Fig. 5 shows the spectrum in coincidence with the 1.43 Mev gamma ray and it was a 4000 minute live time study. Since this is the ground state transition, all gamma rays in cascade should appear in this figure. Because of analysis difficulties of low energy gamma rays, their presence there could not be seen. Of particular interest is the manifest appearance of 3 orders of magnitude of intensity of gamma rays. The first order being the 0.935, 0.744, and 0.511 Mev gamma rays. The second order being the 1.33, 1.24, and 0.84 Mev gamma rays. The third order being the 1.18, 1.07, and the 0.59 Mev gamma rays. The third order gamma rays are dashed in Fig. 5 to indicate that they were weak. The 1.43 Mev gamma ray appears there because of Compton triggering by higher energy sum peaks. The magnitudes of those gamma rays in coincidence with the 1.43 Mev gamma ray are listed in Table V.

A substantial amount of information was derived from the 0.935 and 0.744 Mev coincidence experiments. Fig. 8, a 2000 minute live time run of the 0.935 Mev coincidence spectrum, demonstrates clearly that the 1.24 Mev gamma ray is in cascade with the 0.935 Mev gamma ray. The 1.24 Mev gamma ray being seen in the 0.935 Mev spectrum and not in the 0.744 Mev spectrum established the new level at 3.614 Mev. The absence of the 1.33 and 1.18 Mev gamma rays shows that either these are not in coincidence with the 0.935 Mev gamma ray or that they are very weak. It turned out that the 1.33 Mev gamma ray was not in coincidence, and the 1.18 Mev gamma ray

TABLE V. Intensities of Gamma Rays Coincident with the 1.43 Mev Gamma Ray.

| γ-Ray Mev | #83[a] | #102 | #113B | #247 | Average (rms Error) | |
|---|---|---|---|---|---|---|
| 1.43 | 100 | 100 | 100 | 100 | 100 | |
| 1.33 | 5.6 | 6.0 | 5.9 | 5.7 | 5.8±0.3 | |
| 1.24 | 8.1 | 5.8 | 5.3 | 5.8 | 6.3±2.1 | |
| 1.18 | 1.4 | 2.3 | 0.7 | 1.3 | 1.4±1.1 | weak |
| 1.07 | - | 5.2 | 3.3 | 1.2 | 3.2±2.7 | weak |
| 0.93 | 89.5 | 87.0 | 88.3 | 84.0 | 87.2±2.0 | |
| 0.84 | - | 6.1 | 7.2 | 4.9 | 6.0±1.6 | |
| 0.74 | 84.0[b] | 84.0[b] | 84.0[b] | 84.0[b] | 84.0[b] | |
| 0.63 | - | 2.5 | 2.7 | 2.0 | 2.4±0.5 | weak |
| 0.51 | 58.2 | 62.7 | 51.5 | 67.2 | 59.9±5.8 | |
| Minutes Live Time | 1000 | 2000 | 5000 | 4000 | | |

a. Number indicates run number.

b. Used for normalization.

might have been present but it was too weak to find. In other analyzed runs of this type, the following gamma rays were clearly present: 1.07, 0.847, and 0.63 Mev. This is in addition to the first order magnitude transitions. It will be shown later that these three gamma rays helped to establish the three new energy levels in this isotope. The presence of the 1.07 and 0.847 Mev gamma rays in coincidence with the 0.935 Mev gamma ray implies the existence of a 0.398 Mev gamma ray as a transition between the known levels of 2.766 and 2.369 Mev but it was not seen. Table IV shows the results of these 0.935 Mev coincidence runs.



## 5.3 Revised Decay Scheme of $Mn^{52}$

The revised decay scheme of $Mn^{52}$, as determined from the results of this experiment, is presented in Fig. 10. In the following discussion of the different coincidence runs made and the arguments leading to the establishment of the three new upper levels, specific reference to this figure will not be made but this reference is implied throughout. Only 2 of the 3 new levels are shown since one of the levels (3.74 Mev) was determined by only 1 gamma ray, and this was considered to be only weak evidence for a new level.

Fig. 9, a 1000 minute live time run of the 0.744 Mev coincidence spectrum, does not show the very important gamma ray of 0.63 Mev energy although it appeared in 2 analyzed runs of this type. Since this gamma ray appears in the 1.43, 0.935, and 0.744 Mev coincidence runs, this implies that it feeds the level from which the 0.744 Mev gamma ray issues. This then establishes a possible new level in the decay scheme at 3.74 Mev. Table IV also displays the results of the 0.744 Mev coincidence runs.

The presence of the 3.74 Mev level would yield transitions also to states other than the 3.112 Mev. We would then expect to see the following gamma rays (all Mev and followed by the respective level): 0.77 (2.97); 0.97 (2.77); 1.09 (2.65); 1.37 (2.37); and 2.31 (1.43). It is interesting to note that in each case, except that of the 2.31, the gamma ray is near the energy of a more intense gamma ray already listed and therefore they would not be discernable. It is clearly seen in Fig. 2 that if a gamma ray exists of energy greater than 1.43 it would not be strong and almost impossible to detect with scintillation methods and thus the 2.31 Mev, if it exists, is weak.

The spectrum of those gamma rays in coincidence with the 1.33 Mev gamma ray are shown in Fig. 6. It ran for 5000 minutes live time. This was the most fruitful and interesting run of them all. It alone clearly showed the 0.346 Mev gamma ray. The 1.07 Mev gamma ray seen in Fig. 6 established a new level at 3.832 Mev which was supported by the beta-ray spectrometer group's finding of the 1.46 and 1.21 Mev internally converted electrons. The 1.21 Mev transition was masked in our scintillation studies by the more dominent 1.24 Mev gamma ray, and the 1.46 Mev was lost in the leading edge of the 1.43 Mev main transition. This is an excellent illustration of the utility of using both types of experimental methods, gamma-ray and beta-ray spectrometers, since they can support each other so well. The 1.21 Mev transition coupled with the 1.18 Mev transition seen in the 1.43 Mev gamma ray spectrum support the level assignment at 3.832 Mev. The 1.46 Mev transition also supports the existence of this level.

A series of coincidence runs were made which were designed to display those gamma rays which were feeding the (4+) level at 2.369 Mev. The results of this study supported this revised decay scheme since the following gamma rays appeared to be present besides the 0.744 and 0.511 Mev gamma rays: 1.24, 1.07, 0.847, 0.630, and 0.346 Mev.

The final results of the studies of both the gamma-ray and beta-ray spectrometer groups is given in Table VI. Of significant interest are the weighted averages of the gamma rays and converted electrons seen. Previously the main transition gamma rays were reported as having equal intensities. We have found that the intensities of the 0.935, 0.744, and 0.511 Mev gamma rays have intensities of 87.1%,

TABLE VI. Gamma-Ray Intensities in Decay of $Mn^{52}$

| Gamma Ray Energy(Kev)[a] | Singles | 1.43 Coin. | 1.33 Coin. | 0.935 Coin. | 0.744 Coin. | Internal Conver.[b] | External Conver. | Weighted Average |
|---|---|---|---|---|---|---|---|---|
| 1433.6±0.4 | 100 | 100 | Present | Present | Present | 100 | 100 | 100 |
| 1332±1 | - | 5.8±0.3 | - | - | - | 5.8±0.9 | 4.3±3.4 | 5.8±0.8 |
| 1245.6±0.4 | - | 6.3±2.1 | - | 6.4±1.0 | - | 5.2±1.3 | 6.5±2 | 6.2±1.3 |
| 1214±1 | - | - | - | - | - | 2.8±1.8 | - | 2.8±1.8 |
| 935.1±0.4 | 81.5±4.0 | 87.2±2.0 | - | 85.4±3.1[c] | Present | 86±6.0 | 93±10 | 87.1±3.1 |
| 847.4±0.6 | - | 6.0±1.6 | 2.8±0.3 | 3.9±1.0 | - | 2.5±0.4 | 0.7±0.7 | 2.27±0.4 |
| 743.8±0.3 | 83.2±5.8 | 84.0[d] | - | 84.0[d] | - | 80±8.0 | 83±3 | 84.0[d] |
| 345.74±0.08 | - | - | 0.6±0.3 | - | - | 0.84±0.08 | 1.0±0.2 | 0.86±0.08 |
| Annihilation Radiation | 63.6±6.1 | 59.9±5.8 | Present | 61±10 | 67±10 | - | - | 65.5±8 |
| Weak Transitions[e] | | | | | | | | |
| 2650±30 | 0.08±0.05 | - | - | - | - | - | - | |
| 1463±2 | - | - | - | - | - | 0.3±0.2 | - | |
| 1180±20 | - | <2 | - | - | - | - | - | |
| 1070±20 | - | <4 | <1 | - | - | - | - | |
| 630±60 | - | <3 | <1 | <3 | <5 | - | - | |

a. Beta-ray spectrometer results
b. Based on E2 conversion coefficient
c. From intensity of 1.43 Mev gamma ray
d. Used for normalization
e. Gamma-ray spectrometer results except 1463 Kev

84.0%, and 65.5% respectively. It is emphasized that the energies given are those derived by the beta-ray spectrometer group.

5.4 Comparison of Results of this Paper

Recently Katoh et al.[1] reported their determination of the values of the energy levels of $Cr^{52}$ also using gamma-ray and beta-ray spectroscopy. Table VII and VIII list the results of the three latest independent studies concerning $Cr^{52}$.

TABLE VII. Energy Levels of $Cr^{52}$ (All Kev)

| Mazari et al.[2] and Konijn et al.[3] | Univ. of Colo. Beta-Ray Spectrometer | Proposed Additions[a] | Katoh et al[1] |
|---|---|---|---|
| - | 3831.7 ± 2.0 | - | - |
| - | - | 3800 ± 20 | - |
| - | | 3740 ± 20 | - |
| - | 3613.8 ± 0.5 | - | - |
| - | - | 3480 ± 20 | - |
| 3161 ± 8.0 | - | - | - |
| 3109 ± 7.0 | 3112.1 ± 0.5 | - | 3119.6 ± 0.5 |
| 2965 ± 8.0 | - | - | - |
| 2767 ± 8.0 | 2766.2 ± 0.8 | - | - |
| 2648 ± 8.0 | 2647.6 ± 1.1 | - | - |
| 2368 ± 8.0 | 2368.7 ± 0.7 | - | 2372.8 ± 0.6 |
| 1433 ± 4.0 | 1433.6 ± 0.4 | - | 1434.7 ± 0.8 |

a. See Chapter 6 for details.



TABLE VIII. Comparison of Energy Values of the Main Transition Gamma Rays of $Cr^{52}$

| Katoh et al.[1] | Univ. of Colo. Beta-Ray Spectrometer |
|---|---|
| 1434.7 ± 0.8 | 1433.6 ± 0.4 |
| 938.1 ± 0.4 | 935.1 ± 0.4 |
| 746.8 ± 0.2 | 743.8 ± 0.3 |

It is seen in Table VII that the present work agrees well with the results of Mazari et al.[2] and Konijn et al.[3] Since Mazari et al. used the (p,p') reaction in their determinations they observed low spin states in areas where the decay process is not involved and hence the reason for the blanks in the 'Univ. of Colo.' column of Table VII. Also apparent is the wide diversity (3 Kev in two cases and 1 Kev in another case) in the Katoh et al. results from those in the first two columns. An explanation of a possible reason for this is that from the drawings of their beta-ray spectrometer it appears that they used a solid iron core in their magnet and used magnet current as a field strength indicator. It is believed that at high field strengths they experienced saturation in this core giving non-linear results making their calibrations inaccurate. To obviate this the beta-ray spectrometer used in these studies was designed with coils in the center instead of an iron core.[4]

Some other variations occurred between their results and the results of this paper and an explanation for these could be:

a. The Katoh et al. group used a 20 channel pulse-height analyzer and, hence, did not have the statistical weight in their spectra that is afforded by a 200 channel analyzer.

b. In their spectrum analysis the $Zn^{65}$ gamma-ray pulse-height distribution was used to extract the 1.43 Mev gamma-ray contribution. We found that this energy difference is excessive and does not yield accurate results.

c. They reported the 3 main transition gamma rays as having equal intensity and our results clearly show that this is not the case.

## 5.5 Log ft Values for the Revised Decay Scheme

In order to help in the discussion of spins in the proposed decay scheme, the log ft values are listed in Table IX for the energy levels indicated. They were calculated by using Moszkowski's nomogram,[5] and computing the theoretical (EC/β+) ratio. The calculation of this ratio was performed by finding the (K/β+) ratio[6] for $Mn^{52}$, and then adding appropriate terms[7] for the L and higher shells. The final formula used was:

$$\frac{EC}{\beta^+} = \frac{K}{\beta^+}\left(1 + \frac{L_I}{K} + \left(\frac{L_I}{K}\right)\left(\frac{L_{II}}{L_I}\right) + \left(\frac{L_I}{K}\right)\left(\frac{M}{L_I}\right)\right) \quad (5.1)$$

which gave the result:

$$\frac{EC}{\beta^+} = \frac{K}{\beta^+}(1.095) \quad (5.2)$$

Having the net feeding of a level and the (EC/β+) ratio we can then obtain the log ft value for either the EC or the β+ transitions.



TABLE IX. Log ft Values for $Mn^{52} \rightarrow Cr^{52}$

| Energy Level | Feeding | Leaving | Net | Log ft | |
|---|---|---|---|---|---|
| | | | | β+ | EC |
| 3.832 | 0 | 5% | 5% | energetically prohibited | 6.0 |
| 3.740 | 0 | 3.3% | 3.3% | energetically prohibited | 6.4 |
| 3.614 | 0 | 8.5% | 8.5% | - - | 6.0 |
| 3.112 | 3.3% | 84.9% | 81.6% | - - | 5.5 |

The 3.614 and 3.832 Mev levels have log ft values which are commensurate with allowed electron capture and this could have spins and parities of 5+, 6+, or 7+. Since they both seem to feed 4+ levels, it seems more likely that the spins and parities are 5+ or 6+ rather than 7+. The 3.74 Mev level has a log ft value which is suitable for *1*-forbidden or first forbidden which could yield 5+, 6+, or 7+. The 0.630 Mev which established this level feeds the 6+ level at 3.112 Mev and other levels very weakly if at all. This could indicate that this level has a spin and parity of 7+. The log ft value for the 3.112 Mev level shows it is an allowed transition which is consistent with previously published results. It has been clearly established that this level of $Cr^{52}$ is 6(+) and that the ground state of $Mn^{52}$ is also 6(+). (See Table I).

References for Chapter 5


1. T. Katoh, M. Nozawa, Y. Yoshizawa, and Y. Koh, J. Phys. Soc. Japan, 15, 2140 (1960).

2. M. Mazari, W. W. Buechner, and A. Sperduto, Phys. Rev., 107, 1383 (1957).

3. J. Konijn, B. Van Nooijn, and H. L. Hagedoorn, Physica, 24, 377 (1958).

4. A. A. Bartlett and R. A. Ristinen, Bull. Am. Phys. Soc. 6, II, 240 (1961).

5. S. A. Moszkowski, Phys. Rev., 82, 35 (1951).

6. A. H. Wapstra, G. J. Nijgh, and R. van Lieshout, Nuclear Spectroscopy Tables, (Interscience Publishers, Inc., 1959), p. 65.

7. Ibid, p. 61.




# CHAPTER 6

## Discussion of Results

### 6.1 Branching Ratios of $Mn^{52}$ Decay

The consistency of the previously reported values of $EC/\beta^+$ for the decay $Mn^{52} \rightarrow Cr^{52}$ is seen in Table X.

TABLE X. Branching Ratios of $Mn^{52} \rightarrow Cr^{52}$

| Date | Investigator | Branching ratio reported |
|---|---|---|
| 1946 | Good, Peaslee and Deutsch[a] | $EC/\beta^+ = 1.86 \pm 0.17$ |
| 1954 | Sehr[b] | $EC/\beta^+ = 2.01 \pm 0.22$ |
| 1958 | Konijn et al.[c] | $EC/\beta^+ = 1.99 \pm 0.06$ (exp.) |
| | | $EC/\beta^+ = 2.03 \pm 0.06$ (theor.) |
| 1961 | present | $EC/\beta^+ = 1.50$ |

a. W. M. Good, D. Peaslee, and M. Deutsch, Phys. Rev. 69, 313 (1946).
b. R. Sehr, Z. Physik, 137, 523 (1954).
c. J. Konijn, B. Van Nooijn, and H. L. Hagedoorn, Physica, 24, 377 (1958).

The apparent reason for this anomaly is that the previous investigators relied on the published data of the decay sequence being $6^+$ ($\beta^+$) $6^+$ ($\gamma$) $4^+$ ($\gamma$) $2^+$ ($\gamma$) $0^+$ to the exclusion of all other modes of decay and de-excitation since no other such experimentally found modes had been reported. We will calculate the $EC/\beta^+$ ratio in two different ways. One way yielding results consistent with those previously reported, and another way yielding the results reported in this paper.

The $EC/\beta^+$ can be calculated by using:

$$\frac{EC}{\beta^+} = \frac{(\text{net feeding}) - \beta^+}{\beta^+} \qquad (6.1)$$

By using only the intensity of the 0.744 Mev as the net feeding it is similar to assuming that only this transition is involved in the cascade between 3.112 and 2.369 Mev levels as was the case in earlier experiments. Konijn et al.,[1] Juliano et al.,[2] and El Bedewi and Tadros[3] all list $\beta^+$ as (33%) and EC as (67%) for this decay. Then using $I_{0.744}$ as 100% in equation (6.1) we find:

$$\frac{EC}{\beta^+} = \frac{100 - 33}{33} = 2.03 \qquad (6.2)$$

The above assumption yields a result consistent with the results shown in Table X. However, from Tables V and VI we get 0.744 Mev (84.0%), 0.630 Mev (3.3%), 0.511 Mev (65.5%), and 0.346 Mev (0.9%). The level at 3.74 Mev is not shown on the decay scheme, but it is assumed to be the source of the 0.630 Mev transition to the 3.112 Mev level. The decay scheme also does not show the consequences of such a new level since the 52% electron capture specified would then be decreased in intensity by the amount of the intensity of this 0.63 Mev gamma ray of 3%. The percent of electron capture decay to the 3.112 Mev level would then be 49%. It is important to note here that, although the electron capture decay to the 3.112 Mev level apparently is decreased, the positron decay remains about the same at roughly 33%. This is because the positron decay threshold is at 3.684 Mev and for the 3 new levels considered in this paper it is energetically impossible for positron decay to the 3.74 or the 3.832 Mev levels and very improbable for the 3.614 Mev level. Thus, this revised decay scheme only changes the electron capture contribution to the branching ratio. Again using equation (6.1) we now get:

$$\frac{EC}{\beta^+} = \frac{(84.0 + 0.9 - 3.3) - 1/2\ (65.5)}{1/2\ (65.5)} = 1.50 \qquad (6.3)$$



Thus, the results of this experiment give $EC/\beta^+ = 1.50$ as opposed to about 2.0 as has been previously reported.

6.2 The Results of Hausman et al.[4] Compared to Those of Mazari et al.[5]

In 1952 Hausman et al. reported the results of their reaction study on $Cr^{52}$ of 8 Mev (p,p'). Referring to Table II in Chapter 2 we see that their reaction energy was the highest for a study of the levels of this isotope since the El Bedewi and Tadros report gave only the first excited state energy. It would be expected then that their experiment should yield states of higher energy than any of the other studies since they could surmount higher energy thresholds. Although Hausman et al. did assign three energy levels to their resonance peaks, they hesitated to assign any more but suggested that a designated few might be those of $Cr^{52}$ since all of the others were apparently identified as those of the backing material, etc. They did not list the energies of these resonances but only presented a drawing with peaks indicated by letters. The values of the energies of the inelastically scattered protons suggested as being those of $Cr^{52}$ were taken from this drawing and are shown in Table XI. It is admitted that this is a questionable procedure, but it did lead to interesting results. The levels were calculated by using:[7]

$$Q = E_3\left(1 + \frac{M_3}{M_4}\right) - E_1\left(1 - \frac{M_1}{M_4}\right) - \frac{2\,(M_1 E_1 M_3 E_3)^{\frac{1}{2}}}{M_4}\cos\theta \qquad (6.4)$$

where: 1 refers to the bombarding proton (8 Mev),
3 was taken as the scattered proton, and
4 was taken as $Cr^{52*}$.

The resulting equation used for Table XI is:

$$Q = 1.02\ E_3 - 7.84 + 0.0942\ (E_3)^{\frac{1}{2}} \qquad (6.5)$$

where: $E_3$ is the energy of the inelastically scattered proton.

TABLE XI. Energy Levels of $Cr^{52}$ from Hausman et al.[4]

| Level Assignments (Mev) | $E'_p$ (Mev) | Levels Calculated Q | Levels Adjusted to Mazari et al. | Levels of Mazari et al. |
|---|---|---|---|---|
| 1.46 | 5.86 | 1.64 | 1.43 | 1.432 |
| 2.43 | 4.98 | 2.54 | 2.37 | 2.368 |
| - | 4.68 | 2.87 | 2.67 | 2.648 |
| - | 4.60 | 2.94 | 2.76 | 2.767 |
| 3.01 | 4.41 | 3.14 | 2.96 | 2.965 |
| - | 4.20 | 3.37 | 3.175 | 3.161 |
| - | 3.90 | 3.67 | 3.51[a] | - |
| - | 3.60 | 3.99 | 3.83[a] | - |

a. Listed by Way et al.[6] on p. 40 as 3.46 Mev while 3.83 is not listed therein at all.

There was a noticeable difference between the energies given by Mazari et al. and those calculated. It was thought that the method of using equation (6.4) was in error. Reference was made to the energies given by Mazari et al., and their levels were calculated using (6.4) and ( $\theta = 90°$)[5]. Table XII shows the results and the error was considered as being reasonable. The final equation used for Table XII is:

$$Q = 1.02\ E_3 - 6.38 \qquad (6.6)$$



TABLE XII. Calculation of Levels Given by Mazari et al.

| $E'_p$ (Mev) | Levels Calculated Q (Mev) | Levels Assigned[5] (Mev) |
|---|---|---|
| 6.28 | 0.03 | 0.00 |
| 4.88 | 1.40 | 1.43 |
| 3.95 | 2.35 | 2.37 |
| 3.70 | 2.61 | 2.65 |
| 3.57 | 2.74 | 2.77 |
| 3.38 | 2.93 | 2.96 |
| 3.19 | 3.12 | 3.16 |

Since the use of equation (6.4) then seemed in order, the divergence of the calculated Q's in Table XI from those of Mazari et al. was inexplicable. Noting that equation (6.5) contained a very small quadratic term, it was reasoned that perhaps it would be close to linearity over a limited range. If a linear plot of energy level (Q) versus scattered proton energy were to be made then perhaps a constant factor difference could be found to fit Hausman's results to Mazari's in order to find how well they matched. The linear plot was made of the calculated Q's in column three of Table XI. Taking those levels assigned by Hausman et al. as points of reference, their positions were adjusted vertically downward so as to fall on the values of Mazari et al. Through these three points a straight line was drawn. The Q values listed in column 4 of Table XI are the result. Even though the method employed is somewhat questionable it is seen that agreement with the results of Mazari et al. is very nice. The original line through the calculated Q's before adjustment was indeed linear which supported the original assumption about the size of the quadratic term being small. The lines

were not parallel as was supposed but were closer at the high level end implying that there is a functional and not a constant difference as is easily seen by using a slide rule and Table XI. The net result of this was the finding of two apparently new levels at 3.51 ± 0.03 and 3.83 ± 0.03 with relatively low spin states since they resulted from a particle study.

6.3 The Results of Katoh et al.[8] and $Mn^{52m}$

Recently Katoh et al. reported results of a study of the decay of $Mn^{52m}$, the isomeric state at 5.098 Mev, or 0.390 Mev higher than the ground state of $Mn^{52}$. They report the spin of this level as (2+) or (3+) which is consistent with other results.[2] Some of their other results have been discussed in Chapter 5.

(They also reported seeing gamma rays of 1.33 and 1.2 Mev at intensities estimated at 5% and 3% respectively in coincidence with the 1.43 Mev gamma ray. These apparently are the 1332.0 ± 1.0 Kev (5.8 ± 0.8%) and the 1245.6 ± 0.4 Kev (6.2 ± 1.3%) reported in this paper which supports our findings. However, they reported a very weak gamma ray of 1.73 Mev energy in their singles runs. But, from our studies as shown in Fig. 2 it appears that this 1.73 Mev gamma ray is spurious.)

Their results of the decay of $Mn^{52m}$ included the following gamma rays: 1.52 (2%), 1.37 (missing %), 1.15 (2%), 1.02 (3%), 0.94 (4%), and 0.70 (3%) all Mev. The main decay path is via the emission of a 2.63 Mev positron to the (2+) level at 1.43 Mev (90%). In order to fit these resulting gamma rays into the levels reported by Mazari et al., Katoh et al. suggested that a new level was necessary at 3.67 Mev. In this decay scheme there are apparent misfits in energy of as much as 0.06 Mev.



6.4 Proposed Decay Scheme of $Mn^{52m}$

Recalling that possible low spin states might be present at 3.51 and 3.83 Mev from the report of Hausman et al. it was attempted to fit these levels with the isomeric decay gamma rays reported by Katoh et al. Fig. 16 is such a decay scheme. The 1.02 and 1.15 Mev gamma rays were positioned such that if the 3.83 Mev were a (2+) state then either of these transitions to a (4+) or a (0+) state is probable. These energy levels did not give too good a fit, and the errors assigned to them were used as lower limits at which the levels could be put for a best fit. Thus, the levels in Fig. 16 were assigned the values of 3.48 and 3.80 Mev. The number in parenthesis is the energy difference between levels for comparison purposes. The dashed gamma rays are those expected to be seen in order to complete the cascades to the ground state but which were not reported as having been seen.

Using the intensities as given by Katoh et al. the log ft values for the levels involved were calculated by the use of Moszkowski's nomogram and equation (5.2). The results are given in Table XIII.

TABLE XIII. Log ft Values for $Mn^{52m} \rightarrow Cr^{52}$

| Level Mev | γ-Ray Feeding | Out | Net | Log ft | |
|---|---|---|---|---|---|
| | | | | $\beta^+$ | EC |
| 3.80 | 0 | 5% | 5% | - | 3.82(4.8%) |
| 3.48 | 0 | 3% | 3% | - | 4.40(1.9%) |
| 2.965 | 0 | 2% | 2% | 5.46(1.6%) | - |
| 1.434 | 10% | 100% | 90% | 5.40(88%) | - |

It is seen that the log ft value for the 1.434 level is of the order for an allowed transition which is consistent with

known experimental results. The log ft values for the 3.80 and the 3.48 Mev levels appear to be low which probably means that the intensities given by Katoh et al. were a little high. However, it would seem that if these transitions were allowed then spins and parities for them both could be (1+), (2+), or (3+). Because of the split feeding of a 4+ and a 0+ level, the 2+ assignment seems best for the 3.80 Mev level. Since a 0.83 Mev gamma ray was not reported, then the 3.48 Mev level might best be 3+ since the 2.65 Mev level is not populated from this state.

The level at 2.965 Mev has been tentatively assigned the spin and parity of (2+) by Van Patter. The log ft values indicate that the decay to the 2.965 Mev level could be an allowed transition to yield either (1+), (2+), or (3+) for spin and parity and therefore this data could support the assignment of Van Patter of (2+).

It is seen in Fig. 16 that the 3.83, 3.74, and 3.614 Mev levels are apparently not populated as would be expected. It is interesting also to note that the 3.161 Mev level is not populated in either the $Mn^{52}$ or the $Mn^{52m}$ decay. An explanation of this could be that it is a negative parity state and hence requires a first forbidden beta branch.

## 6.5 $V^{52} \rightarrow Cr^{52}$ Beta Decay

K. Way et al.[6] suggested a possible experiment with $V^{52}$ as a means of determining which of the $Cr^{52}$ levels are indeed 2+. The ground state of $V^{52}$ is 2+ and allowed beta-decay transitions would populate the 2+ levels of $Cr^{52}$ most strongly. This investigation is presently underway using 98% chemically pure $V^{51}$, irradiated by thermal neutrons from a Ra-Be source enclosed in a paraffin box. As yet, no definitive results can be reported.



## 6.6 Theoretical Points of Interest

The pure vibrational spectrum[9] of an even-even nucleus is characterized by bands of states separated by energy gaps. The sequence being: ground state (0+); first excited state (2+); second, third, and fourth excited states in a band with some arrangement of (0+, 2+, and 4+); and the fifth through ninth excited states in a higher band of spin and parity (0+, 2+, 3+, 4+, 6+) not respectively. A pure rotational band on the other hand is characterized by quadrupole transitions and a level sequence up from the ground state of (0+, 2+, 4+, 6+) in a ladder type diagram but the energy gaps between levels are much smaller than those for the vibrational spectrum. The rotational spectrum results from nuclei possessing a nonspherical equilibrium shape giving rise to a spectrum like that of a polar molecule (dumbbell). The closed shell nuclei possess spherical equilibrium[9-11] and thus can be described by the addition of a harmonic oscillator term to the Hamiltonian. Spherical symmetry allows the maximum interplay of short range nuclear cohesive forces thus yielding vibrations of high frequency and large energy gaps in the spectrum. When nuclei have unfilled shells the intrinsic forces of the closed shell core are not as effective on the nucleons in the outer shell and the larger the number in this unfilled shell, or mid-range between closed shells, the less effective are these forces. These excess nucleons generate the nuclear deformation and their asymmetric motion can tend to polarise the closed shell core giving rise to higher values of deformation than expected.[9] The large moment of inertia attendant to large nonspherical equilibrium shapes allows smaller values of angular momentum to arise from energy quanta. Thus, the nuclei with many

nucleons in this unfilled shell should display almost pure rotational spectra and the nuclei with the larger A showing smaller energy gaps. This is seen to be the case for the $150<A<190$ and $A>222$ elements.[9] For the $40<A<150$ region this latter effect is not pronounced and large deformations do not occur.

A criterion to tell if a given nucleus would possess a rotational spectrum was calculated by Temmer and Heydenburg.[12] They took the rough criterion given by Bohr and Mottelson that a rotational spectrum should have a correspondence to $(E = J(J+1)\hbar^2/2I)$ and they calculated, for a rotational spectrum, the energy of the first excited state to be:

$$E(^1 2+) < \frac{9.22 \times 10^5}{A^{5/3}} \text{ Kev} \qquad (6.7)$$

Van Nooijn et al.[13] investigated $Ti^{48}$, which has 2 protons outside of a closed shell and 2 neutron holes, and found its levels and parities to be:

| | | | |
|---|---|---|---|
| $_{22}Ti^{48}_{26}$ | $0.986 \pm 0.003$ | $2+$ | (all Mev) |
| | $2.300 \pm 0.005$ | $4+$ | |
| | $3.240 \pm 0.015$ | $4+$ | |
| | $3.340 \pm 0.006$ | $6+$ | |

They calculated the criterion for this isotope to get $E(^1 2+) < 1.46$ Mev and concluded that $Ti^{48}$ must have rotational level spacing since $E(^1 2+)$ was 0.986 Mev. However, it must be recalled that rotational spectra are usually seen only in isotopes of $150<A<190$ and is not to be expected in isotopes of $A \sim 48$. A calculation for the case of $Cr^{52}$ yielded $E(^1 2+) < 1.28$ Mev and $Cr^{52}$ has $E(^1 2+) = 1.433$ Mev it would appear that a vibrational spectrum would be favored. A comparison of their energies normalized to the first excited state shows:



| $_{22}Ti^{48}_{26}$ | | $_{24}Cr^{52}_{28}$ |
|---|---|---|
| 1.00 | $2+$ | 1.00 |
| 2.33 | $4+$ | 1.66 |
| 3.29 | $4+$ | 1.93 |
| 3.39 | $6+$ | 2.17 |

These results show a marked difference and one wonders at the connection between the Temmer and Heydenburg criterion (if it is applicable for $A \sim 50$) and the above table.

An interesting experiment to compare this result with is to investigate the levels of $Ti^{44}$ since it has 2 protons and 2 neutrons outside of a closed shell. In addition, a comparison of $Ca^{44}$ with all of these would yield valuable information since $Ca^{44}$ has 4 excess nucleons (neutrons), $Cr^{52}$ has 4 excess nucleons (protons) and $Ti^{44}$ has 4 excess nucleons (2 protons and 2 neutrons). Using equation 6.7 again for $Ca^{44}$ to see what results, the criteria yield $E(^1 2+) < 1.75$ Mev for a rotational spectrum. Since $E(^1 2+) = 1.16$ Mev for this isotope it appears that it would have a rotational spectrum too if the criterion is applicable.

Mallman[14] presents a graph of energy of the first odd-parity state as a function of the mass number A. He states that Morinaga[15] has found the first odd-parity state of even-even nuclei to have predominantly a spin of 3 and appear near the line

$$E = \frac{67}{A^{3/4}} \text{ Mev} \qquad (6.8)$$

(a semi-empirical formula which is used to describe the separation of two mass parabolas in even A nuclei). Alder et al.[9] state that the odd parity collective vibrations of lowest energy are expected to be of octupole character ($I = 3$). In even-even nuclei this is the one phonon excitation. The two phonon excitation of octupole vibrations give rise to states

of I = 0+, 2+, 4+, and 6+. $Ca^{40}$ which is magic-magic has a 3- state at 3.73 Mev. $A^{40}$ has a 3- state at 4.21 Mev and it has 2 holes and 2 excess protons. $Ce^{140}$ has a 3- state at 2.42 Mev and it has 8 protons outside of a closed shell of 50 and could be expected to yield a spectrum similar to that of $Cr^{52}$. The level at 3.161 Mev in $Cr^{52}$ has been tentatively assigned the spins and parities of (1-, 2-, 3-) for reasons already given. The energy level falls nearly on the line given in equation 6.8. Systematically it appears then that the 3.161 Mev could be the first odd parity state of $Cr^{52}$.

In conclusion, it appears that the spectrum of $Cr^{52}$ is not a pure j-j coupling spectrum, nor is it a pure vibrational spectrum, nor is it a pure rotational spectrum. Rather, it is a very complex combination of several effects, and at this time there is active interest in creating a model to explain such nuclei as $Cr^{52}$.

## References for Chapter 6


1. J. Konijn, B. Van Nooijn, and H. L. Hagedoorn, Physica, 24, 377 (1958).
2. J. O. Juliano, C. W. Kocher, T. D. Mainan, A.C.G. Mitchell, Phys. Rev., 113, 602 (1959).
3. F. A. El Bedewi and S. Tadros, Nuclear Phys., 6, 434, (1958).
4. H. J. Hausman, A. J. Allen, J. S. Arthur, R. S. Bender, and C. J. McDole, Phys. Rev. 88, 1296 (1952).
5. M. Mazari, W. W. Buechner, and A. Sperduto, Phys. Rev. 107, 1383 (1957).
6. K. Way, R. W. King, C. L. McGinnis, R. van Lieshout, Nuclear Level Schemes, AEC TID-5300, GPO, 1955.
7. R. D. Evans, The Atomic Nucleus, (McGraw-Hill Book Co., Inc., New York, 1955) p. 411.
8. T. Katoh, M. Nozawa, Y. Yoshizawa, and Y. Koh, J. Phys. Soc. Japan, 15, 2140 (1960).
9. K. Alder, A. Bohr, T. Huus, B. Mottelson, and A. Winther, Rev. Mod. Phys. 28, 4, 432 (1956).
10. C. E. Mandeville, D. M. Van Patter, W. C. Porter, M. A. Rothman, and C. P. Swann, Air Force Office of Scientific Research Report, AFOSR-TR-59-28 (1959).
11. L. S. Kisslinger and R. A. Sorensen, Kgl. Danske Videnskab. Selskab, Mat.-fys. Medd., 32, No. 9 (1960).
12. G. M. Temmer, and N. P. Heydenburg, Phys. Rev. 99, 1609 (1955).
13. B. Van Nooijn, J. Konijn, A. Heyligers, J. F. Vander Brugge, and A. H. Wapstra, Physica 23, 753 (1957).
14. C. A. Mallmann, A/CONF. 15/1, 14, P/1971 (1958).
15. H. Morinaga, Phys. Rev., 103, 503 (1956).

APPENDIX A

## Construction of Intrinsic Efficiency Curves for NaI(Tl) Crystals

Consider a monoenergetic gamma-ray source. It has a given emitted flux at any known time. Of the total number of gamma rays emitted, only a small fraction lie in the solid angle subtended by the crystal and are absorbed by it. This fraction is called "total absolute efficiency." Of the gamma-ray energy converted into photons in the crystal only another small fraction fall under the photoelectric effect curve.

The area under the full curve of counts versus pulse height is proportional to the total number of distinct gamma rays that were transformed in the crystal and is thus proportional to the probability of the event occurring. If a spectrum contains only two gamma rays, then the ratio of their two total areas is a measure of the relative probability of the events occurring and is thus a measure of the relative intensity of these two radiations.

The ratio of the area under an ideal photoelectric effect peak to the total area is a constant for a given crystal and gamma ray. For instance, Table A-I shows such a relationship for 2 different NaI(Tl) crystals used in the Nuclear Physics Laboratory, University of Colorado.

TABLE A-I. Photoelectric peak area/total area ratios.

| Source | γ-Ray Mev | (3" x 3") | (3-3/4" x 3") |
|---|---|---|---|
| $Cs^{137}$ | 0.661 | 0.502 | 0.522 |
| $Co^{60}$ | 1.17 | 0.326 | 0.394 |
| $Na^{22}$ | 1.28 | 0.292 | 0.324 |

In general, we see that a larger crystal allows more of the Compton effect photons to be recovered, thereby increasing the ratio.



In practice it is much easier to measure the height and width of the photo-peak area than the area of the total. Thus, we seek a way of comparing the relative intensity of gamma rays by comparing the areas of their photo-peaks. The relationship used is:

$$N_p = \varepsilon P \Omega N_o \qquad (A.1)$$

where (1) $N_p$ is the number of $\gamma_i$ in the photoelectric peak.

(2) $\varepsilon$ is the total efficiency for source used.

(3) P is the ratio of photo-peak area/total area.

(4) $N_o$ is the total flux of $\gamma_i$ from the source.

(5) $\Omega$ is the solid angle subtended by the crystal.

We usually plot the number of counts or gamma rays versus channel number on semi-log paper thereby converting the gaussian curve of standard distribution of the photo peak into a parabola. We then use the width at one half maximum as the width of a rectangle whose height is that of the apex of the parabola of the photo-peak. Then $N_p = h\, W_{\frac{1}{2}}$ is the area of the photo-peak and also a measure of the probability of the gamma ray occurring. Then, using (A.1),

$$N_{o_i} = \frac{h\, W_{\frac{1}{2}}}{\varepsilon_i P_i \Omega_i} \qquad (A.2)$$

is a measure of the true intensity of gamma ray $\gamma_i$. Since $(\varepsilon_i)$ is difficult to obtain we can use the relative intensities of two different gamma rays appearing in the same nucleus.

$$\frac{N_{o_1}}{N_{o_2}} = \frac{(h\, W_{\frac{1}{2}})_1 / (\varepsilon P)_1}{(h\, W_{\frac{1}{2}})_2 / (\varepsilon P)_2} \qquad (A.3)$$

The quantity $(\varepsilon P)_1$ is called the "total intrinsic efficiency" of the gamma ray-crystal-geometry used. Since

the solid angle cancelled out it will be a parameter for the curve. Let us denote this by $\alpha(1)$. Then

$$I_{rel.} = \frac{(h\,W_{\frac{1}{2}})_1\,\alpha(2)}{(h\,W_{\frac{1}{2}})_2\,\alpha(1)} \qquad (A.4)$$

To implement this result we use the relative intensity of two gamma rays from their published decay schemes. Then

$$\frac{\alpha(2)}{\alpha(1)} = \text{constant} \qquad (A.5)$$

is determined by analyzing known sources, to find the appropriate h and $W_{\frac{1}{2}}$ with the larger gamma ray placed near channel 150 on the analyzer so as to obtain optimum statistics. Then to obtain a curve of intrinsic efficiency versus gamma-ray energy we assume a value for $\alpha(1)$ in equation (A.5) in order to determine $\alpha(2)$ for one isotope which yields two points for the curve. Each isotope used yields two points for each unique combination of gamma rays. The assumed values are readjusted until all of the points for the various isotopes used fall in a rather smooth curve. Some representative relative intensities using published data are shown in Table A-II.

TABLE A-II. Relative Intensities of Selected Gamma Rays.

| Source | γ-Rays Mev | Relative Intensity |
|---|---|---|
| $Na^{22}$ | 1.274<br>.511 | $\frac{I_{0.511}}{I_{1.28}} = 1.796$ |
| $Co^{60}$ | 1.17<br>1.33 | $\frac{I_{1.33}}{I_{1.17}} = 1.0$ |



Table A-III below displays the ratio $\alpha(2)/\alpha(1)$ for the indicated sources which were used to construct Fig. 11.

TABLE A-III. Relative intrinsic Efficiencies of known gamma rays for a (3-3/4" x 3") NaI(Tl) crystal.

| Source | $Na^{22}$ | $Co^{60}$ | $Sc^{46}$ |
|---|---|---|---|
| Ratio | $\frac{\alpha(0.511)}{\alpha(1.28)} = 1.76$ | $\frac{\alpha(1.17)}{\alpha(1.33} = 1.06$ | $\frac{\alpha(0.885)}{\alpha(1.12)} = 1.12$ |

| Source | $Pr^{144}$ | $V^{48}$ |
|---|---|---|
| Ratio | $\frac{\alpha(2.18)}{\alpha(0.697} = 0.482$ | $\frac{\alpha(2.25)}{\alpha(1.32)} = 0.765$ |
| | | $\frac{\alpha(0.986)}{\alpha(1.32)} = 1.46$ |
| | | $\frac{\alpha(0.511)}{\alpha(1.32)} = 1.71$ |

Fig. 12 was constructed from a similar table for a (2" x 2") crystal as shown in Table A-IV below.

TABLE A-IV. Relative intrinsic efficiencies of known gamma rays for a (2" x 2") NaI(Tl) crystal.

| 1" Source to crystal distance | | | |
|---|---|---|---|
| Source | $Na^{22}$ | $Co^{60}$ | $Pr^{144}$ |
| Ratio | $\frac{\alpha(1.28)}{\alpha(0.511)} = 0.355$ | $\frac{\alpha(1.33)}{\alpha(1.17)} = 0.89$ | $\frac{\alpha(2.18)}{\alpha(0.694)} = 0.303$ |

| 1-1/2" Source to crystal distance | | |
|---|---|---|
| Source | $Pr^{144}$ | $Zn^{65}$ |
| Ratio | $\frac{\alpha(2.18)}{\alpha(0.694)} = 0.314$ | $\frac{\alpha(1.11)}{\alpha(0.511)} = 0.436$ |

In Fig. 11 the 40 cm line was positioned relative to the experimental 14 cm line by analysis of Heath's curves. The 30 cm line was then interpolated into position. In Fig. 12 the 1" and 1-1/2" are experimental results and the 3" line was extrapolated again based on Heath's work.



APPENDIX B

Variation in Shape of a Gamma Ray as a Function of Analyzer Gain or Channel Number

Miller and Snow[12] have shown that theoretical calculations of the gamma-ray absorption process have reached a state as to be able to fit the experimentally determined gamma-ray pulse height spectrum quite nicely. Practically speaking, it is necessary to have at hand during spectrum analysis a catalogue of gamma rays of various energies, and each of these positioned and plotted for convenient channel increments. With the above calculations performed we now have a technique to construct such catalogues appropriate for selected crystals and geometries.

It is found that as the multi-channel pulse height analyzer gain is changed the pictorial presentation of the gamma-ray shape also changes. The gamma-ray photo-peak broadens as the gain is increased and the gamma-ray photo-peak is moved to the right, toward higher channel numbers. Fig. 13 illustrates this change for the $Zn^{65}$ isotope using a (3-3/4" x 3") NaI(Tl) crystal at 14 cm source to crystal distance. This effect is due to the resolution of the spectrometer being determined primarily by the crystal-photomultiplier tube combination and is a constant for a gamma ray of a given energy. The definition of resolution, equation (3.1), shows that as the amplifier gain is changed the resolution is not changed since the resolution is independent of this effect. This can be seen graphically by reference to Fig. 15, showing an analyzer calibration curve. First, select any gamma-ray energy on the ordinate and also a $\Delta E_{1/2}$ centered on this selected energy. Since this relationship is constant, draw two imaginary horizontal lines from the ends of $\Delta E_{1/2}$ to intersect the analyzer

calibration curve. As the analyzer gain is changed so does the slope of this intersected portion of the curve. The slope decreases as the gain is increased and a given energy point is moved to the right. The two parallel lines intercept an increasing number of channels as the slope is decreased which indicates peak broadening. There is no apparent remedy for this. The effect is, however, that in the subtraction procers during analysis (Chapter 4) precise curves are needed for precise subtraction. For each possible gain setting a complete catalogue of sample gamma-ray shapes is required. For continuity, just as set geometries are required to eliminate some variables, set gains are required. so that a catalogue of gamma ray shapes can be made and used throughout the analysis.

During the progress of the experiment such a catalogue was made for our equipment, although it was extremely modest in size.

Early in the experiment it was thought that the Compton distribution was flat from the crest of the leading edge all the way to the left. Observation of $Zn^{65}$ with its relatively uncluttered spectrum, $Mn^{54}$, $K^{42}$, and plates in the literature yielded convincing evidence that there was a slight drop off to the left as seen in the analyzed coincidence drawings in the body of this paper. An effort was made to use all of the appropriate standard calibration sources available in order to construct the above mentioned catalogue. Each source was positioned at various channels (gain) and plotted. We then had a record of variation in shape of one isotope's curves as a function of gain, which yielded the variation in gamma-ray shape (at a constant channel) as a function of energy. The dashed curve in Fig. 13 indicates how interpolation can be used to obtain a desired gamma-ray curve for a specific channel if none is at hand.

With this study as background we made a catalogue of curves for the "set" gains used in this experiment. It is felt that this contributes a great deal to the accuracy and reproducibility of this analytical technique.

APPENDIX C

Variation in Shape of a Gamma Ray when it is the Sum of Two Other Gamma Rays.

On page 3-6 it was mentioned that source to c[illegible] distance had a marked effect on the contribution of sum peaks to a spectrum. However, the possibility exists that choice of geometry may not be one of the luxuries available to the investigator and a detailed knowledge of the shape of a sum peak may be extremely useful. It was suggested that such an investigation be undertaken. Again the magnitude of the inquiry was small but the results were very satisfying. $Na^{22}$ was selected because of its prominent annihilation peak and the separation in energy of the two main gamma rays indicated that their sum peak at 1.79 Mev would be relatively isolated. Three runs were analyzed and the results shown in Fig. 14. Restriction of page size demanded that the two peaks of .511 Mev and 1.28 Mev not be shown in order to allow the sum peak to be made larger. A superposition of a $K^{42}$ (1.53 Mev) gamma-ray curve is shown to indicate the type of variation existing. It is seen that the Compton effect leading edge is very much inflated and the photo-peak reduced.

It is known that real gamma rays of high energy have a small (peak/total area) ratio (See Heath's Catalogue) as does this sum peak. But, the visible difference between these two curves arises from a narrowed half width, and a higher Compton in the sum peak curve. The Compton leading edge has taken on an almost circular shape. It is assumed that the Compton contribution drops slightly as the energy is decreased as do the real gamma rays.



APPENDIX D

Calibration Procedure for the Model 302 Universal Coincidence Circuit.

As discussed in paragraph 3.5, the calibration procedure for the gating discriminator is one of the most critical steps in the coincidence experiments. Chapter 5 lists the energies of the gamma rays seen in $Mn^{52}$ as found by the beta-ray spectrometer research group. These energies are close to the energies originally reported by the beta-ray spectrometer group early in the experiment. Having relatively good values for the energies of the first order gamma rays of this isotope early in the experiment, we had the option of using internal calibration of our instruments for the gamma-ray spectrometer, or external calibration using known calibration sources. Fig. 15 shows a calibration curve using internal calibration. Regardless of whether external or internal calibration is used the procedure to be discussed is unchanged. Fig. 15 is for illustration purposes only and the discriminator voltages listed were not used in any experiment.

The analyzer calibration curve is made by setting the 200-channel pulse-height analyzer at an appropriate gain such that the desired energy range is covered by the 200 channels. Then the #2 counter is used to record coincidence-singles at this gain setting and geometry desired. Assuming that this singles run has been plotted, it is desired that the area between channels 130 and 150 be investigated with the center being at channel 140. This area could contain a gamma ray or any interesting portion of the plotted spectrum desired to be investigated. The energy on the ordinate shows channel 140 to correspond to 1.90 Mev.

APPENDIX C

Variation in Shape of a Gamma Ray when it is the Sum of Two Other Gamma Rays.

On page 3-5 it was mentioned that source to crystal distance had a marked effect on the contribution of sum peaks to a spectrum. However, the possibility exists that choice of geometry may not be one of the luxuries available to the investigator and a detailed knowledge of the shape of a sum peak may be extremely useful. It was suggested that such an investigation be undertaken. Again the magnitude of the inquiry was small but the results were very satisfying. $Na^{22}$ was selected because of its prominent annihilation peak and the separation in energy of the two main gamma rays indicated that their sum peak at 1.79 Mev would be relatively isolated. Three runs were analyzed and the results shown in Fig. 14. Restriction of page size demanded that the two peaks of .511 Mev and 1.28 Mev not be shown in order to allow the sum peak to be made larger. A superposition of a $K^{42}$ (1.53 Mev) gamma-ray curve is shown to indicate the type of variation existing. It is seen that the Compton effect leading edge is very much inflated and the photo-peak reduced.

It is known that real gamma rays of high energy have a small (peak/total area) ratio (See Heath's Catalogue) as does this sum peak. But, the visible difference between these two curves arises from a narrowed half width, and a higher Compton in the sum peak curve. The Compton leading edge has taken on an almost circular shape. It is assumed that the Compton contribution drops slightly as the energy is decreased as do the real gamma rays.



The Model 202 coincidence circuit is now switched from "upper-lower" discriminator selection to "lower-battery bias" discriminator setting. The former is a differential discriminator setting which allows two discriminators to be set independently to define the voltage window. The latter is an integral discriminator using the lower level discriminator but the upper discriminator grid is biased relative to that of the lower by a battery so that a constant window is had as the lower level discriminator is used as a single channel pulse-height analyzer. We found that a voltage bias of 1-1/2 volts was optimum since small peaks were then well defined.

The output of this single channel PHA is fed into a scaler. To find the position of the first order gamma rays of our isotope ($Mn^{52}$ in this case) we set the discriminator high so that few counts are recorded. We then pass down the voltage scale until the change of the counting rate indicates a definite leading edge of a gamma-ray pulse distribution. A voltage in this area is selected as reference and the counts are recorded for 5 or 10 seconds, depending on the source strength. The discriminator is then reduced by 1-1/2 volts to a new setting and a count is made and recorded. This is continued until the maximum of the peak is clearly passed. The energy in this illustrative case is 1.43 Mev and the peak has its center at 33-1/2 volts. The abscissa of Fig. 15 is now relabeled to read volts and this point of 1.43 Mev at 33-1/2 volts is plotted thereon. This process is continued with the result that 0.935 Mev centers at 21-1/2 volts, 0.744 Mev centers at 17 volts, and the annihilation quanta of 0.511 Mev centers at 11-1/2 volts. This curve is drawn and extended passed the 1.90 Mev area in which we are interested.

The plotted spectrum of the #2 counter shows that the area of interest has upper and lower energies of 1.78 Mev to 2.04 Mev. These energies are drawn on the discriminator curve and found to be from 41.5 volts to 48.0 volts.

The differential discriminators are now used and these voltages are set in them.

This procedure is obvious and not at all difficult to perform. It allows the investigator to choose the area to be investigated precisely and to set the discriminators just as precisely. The discriminator itself can drift as a result of variation in room temperature, or the amplifier which feeds this discriminator can drift. Both effects are possible sources of serious error and room temperature stabilization is necessary for precise work.

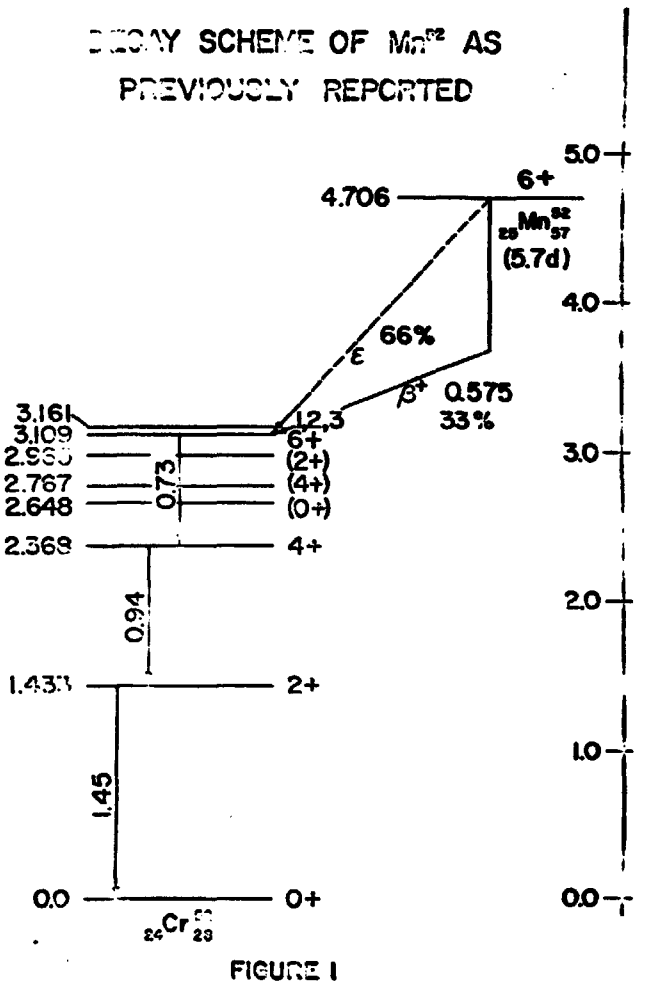


FIGURE I

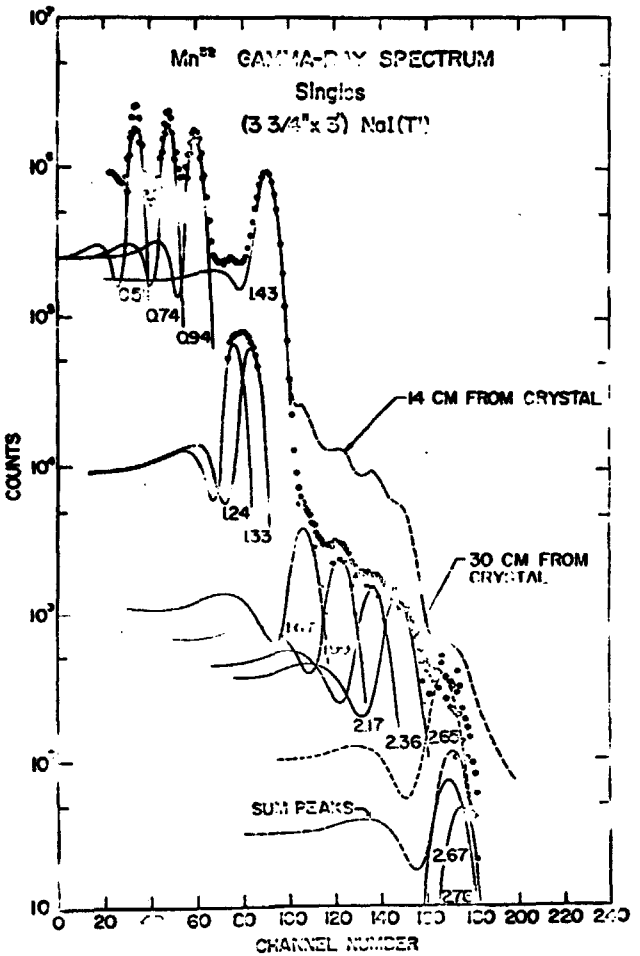
Mn⁵⁴ GAMMA-RAY SPECTRUM
Singles
(3 3/4"x 3") NaI(Tl)
14 CM FROM CRYSTAL
30 CM FROM CRYSTAL
SUM PEAKS
0.51
0.74
0.94
1.43
1.24
1.33
2.17
2.36
2.65
2.67
COUNTS
CHANNEL NUMBER
0
20
60
100
120
140
200
220

FIGURE 2

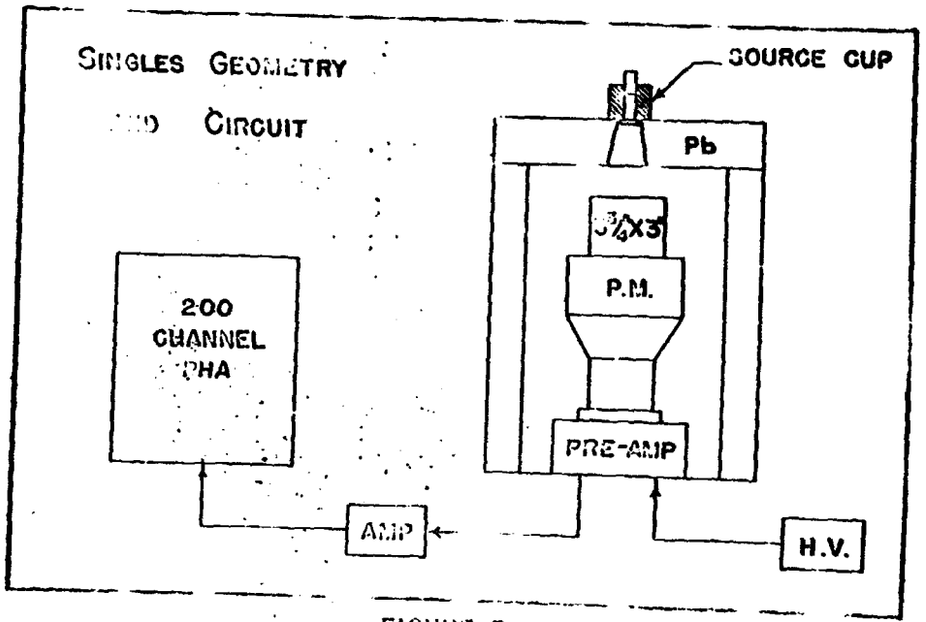
SINGLES GEOMETRY
CIRCUIT
SOURCE CUP
Pb
3"X3"
P.M.
PRE-AMP
200
CHANNEL
PHA
AMP
H.V.

FIGURE 3

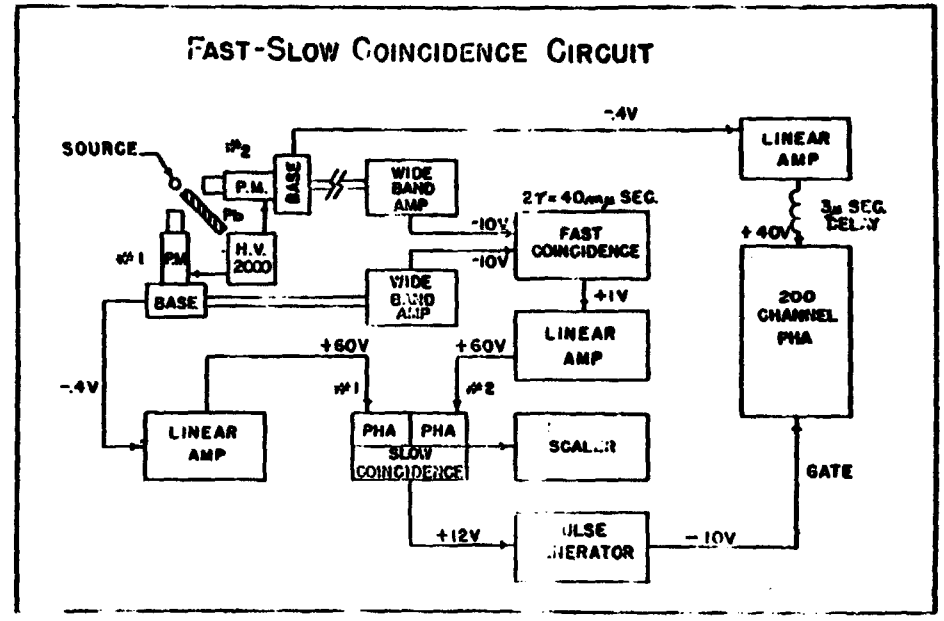
FAST-SLOW COINCIDENCE CIRCUIT
SOURCE
#2
P.M.
BASE
Pb
H.V. 2000
#1
P.M.
BASE
WIDE BAND AMP
WIDE BAND AMP
-10V
-10V
FAST COINCIDENCE
2τ = 40mμ SEC.
+1V
LINEAR AMP
-4V
LINEAR AMP
3μ SEC. DELAY
+40V
200 CHANNEL PHA
+60V
+60V
#1
#2
-4V
LINEAR AMP
PHA
PHA
SLOW COINCIDENCE
SCALER
GATE
+12V
PULSE GENERATOR
-10V

FIGURE 4

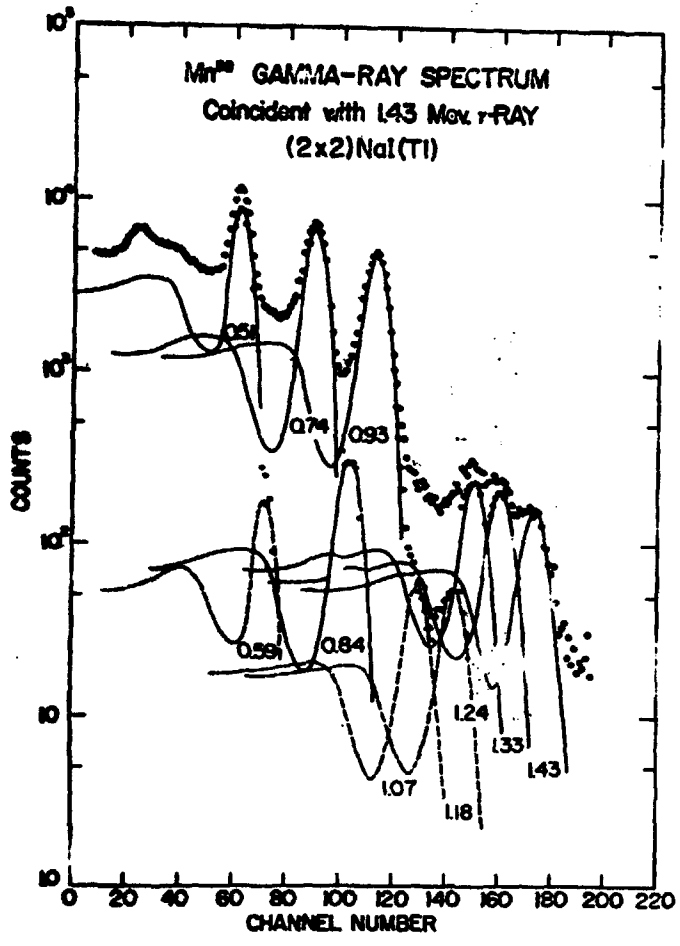


FIGURE 5

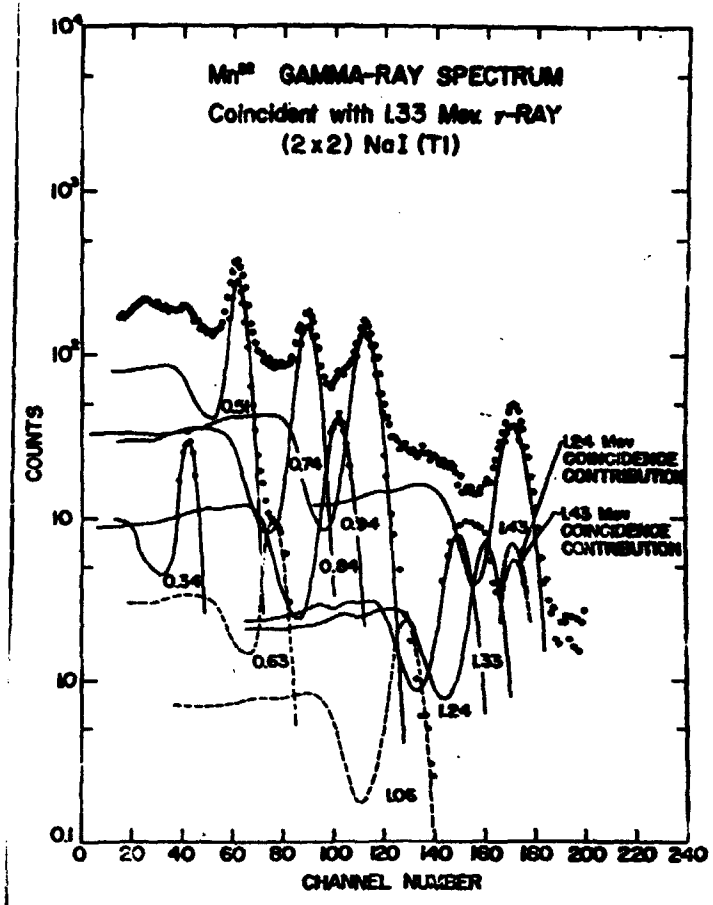


FIGURE 6

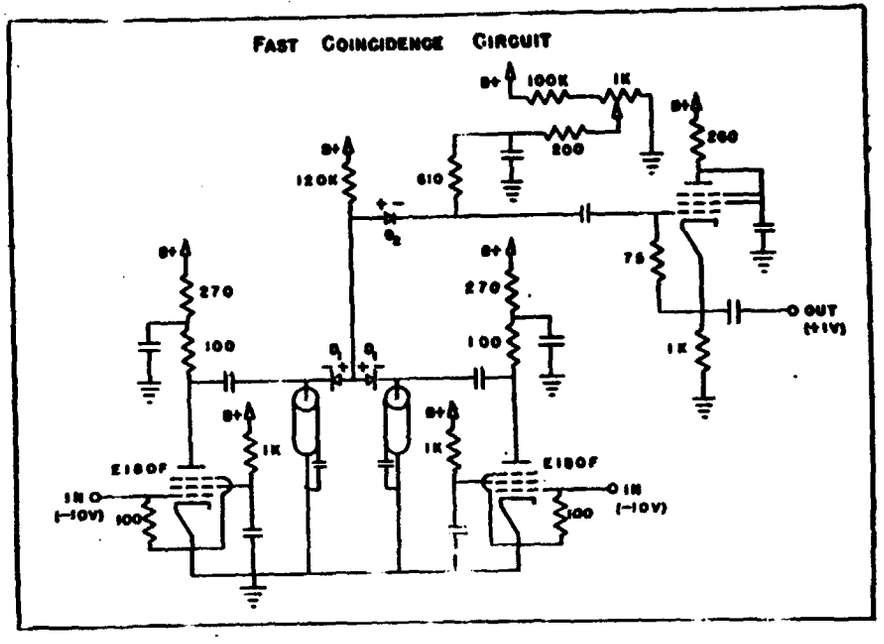
FAST COINCIDENCE CIRCUIT
B+
100K
1K
200
250
120K
610
270
100
75
OUT
(+1V)
1K
E180F
IN
(-10V)
IN
(-10V)

FIGURE 7

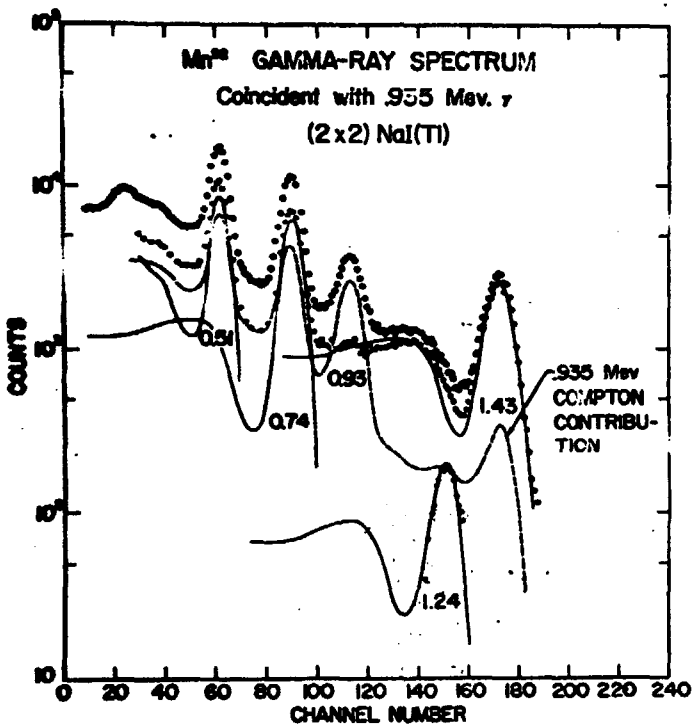


FIGURE 8

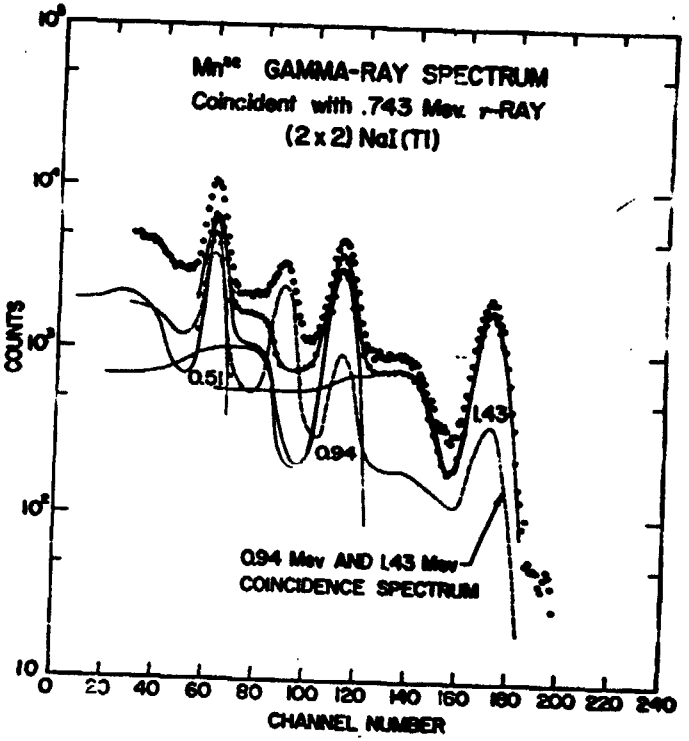


FIGURE 9

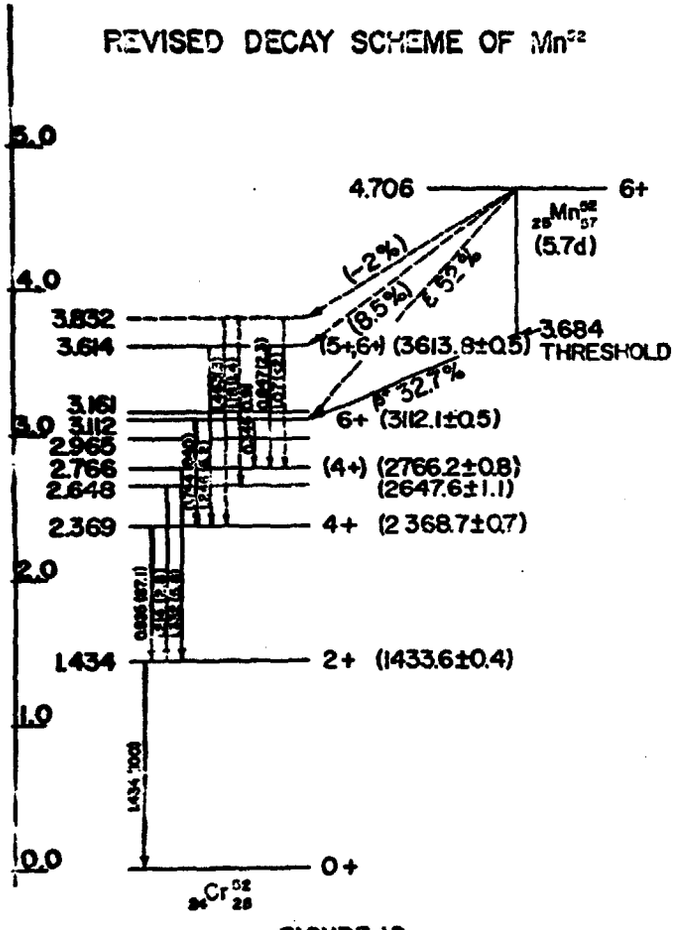


FIGURE 10

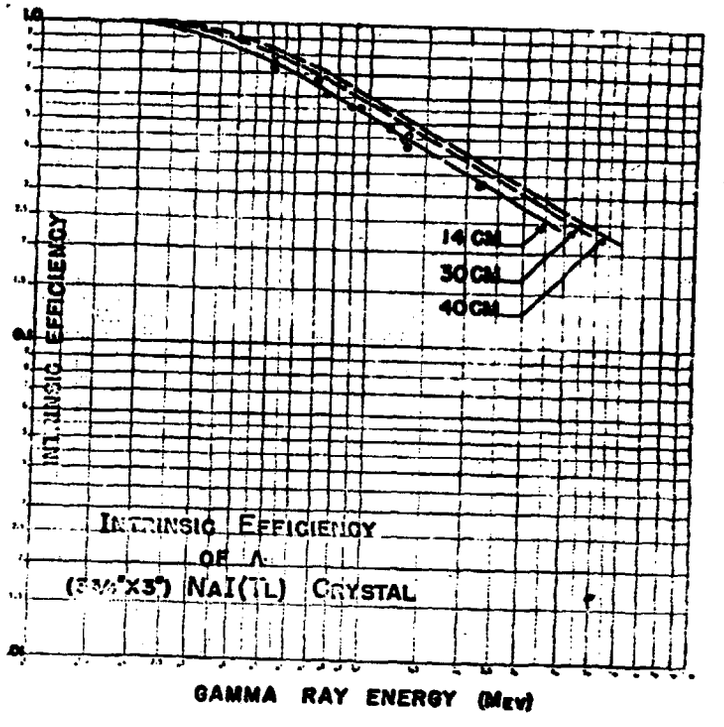


FIGURE 11

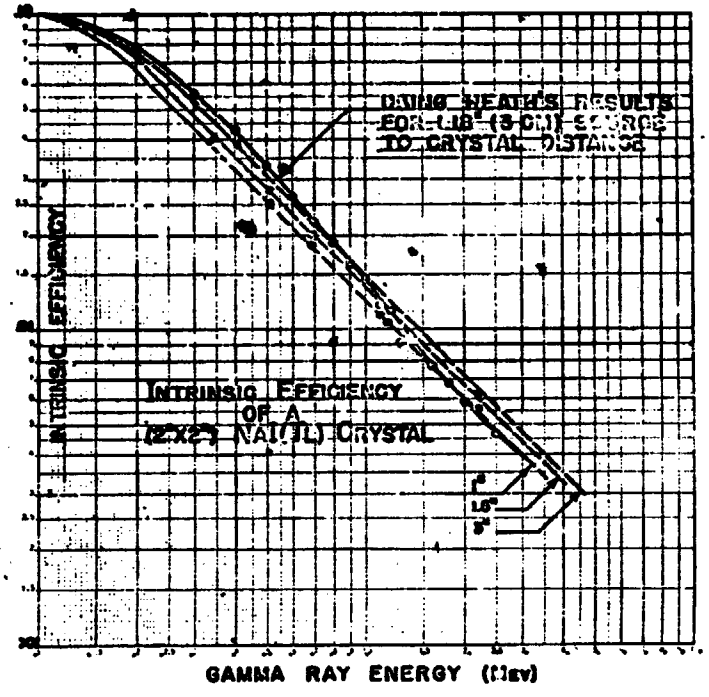
INTRINSIC EFFICIENCY
GAMMA RAY ENERGY (Mev)
INTRINSIC EFFICIENCY OF A (2"X2") NaI(Tl) CRYSTAL

FIGURE 12

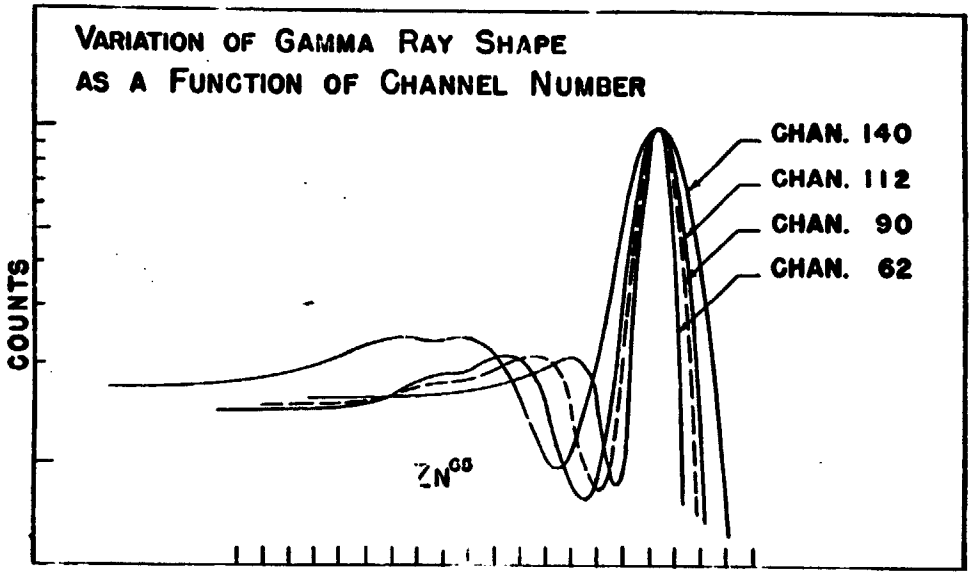
VARIATION OF GAMMA RAY SHAPE
AS A FUNCTION OF CHANNEL NUMBER
CHAN. 140
CHAN. 112
CHAN. 90
CHAN. 62
COUNTS
$ZN^{65}$
CHANNELS

FIGURE 13

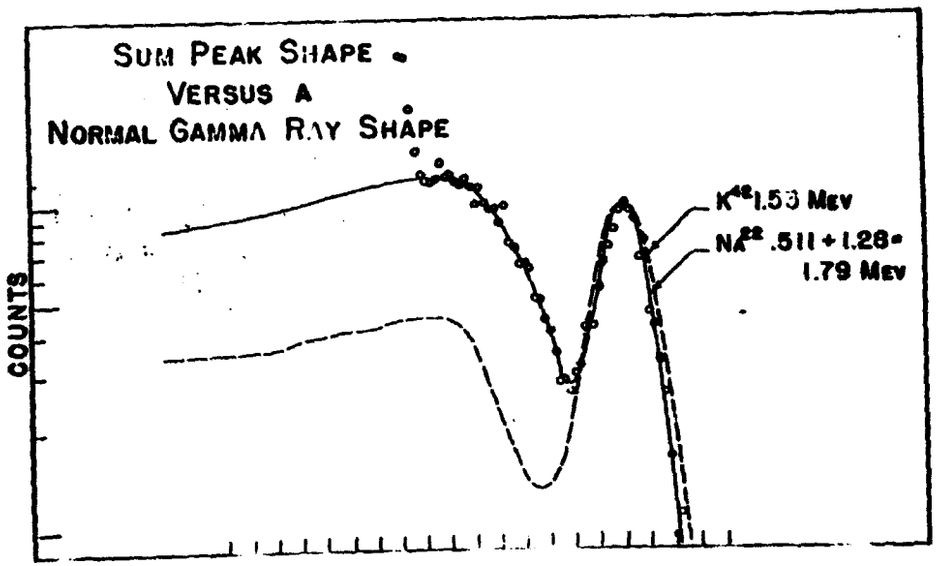
SUM PEAK SHAPE
VERSUS A
NORMAL GAMMA RAY SHAPE
K42 1.53 Mev
Na22 .511 + 1.28 =
1.79 Mev
COUNTS
CHANNELS

FIGURE 14

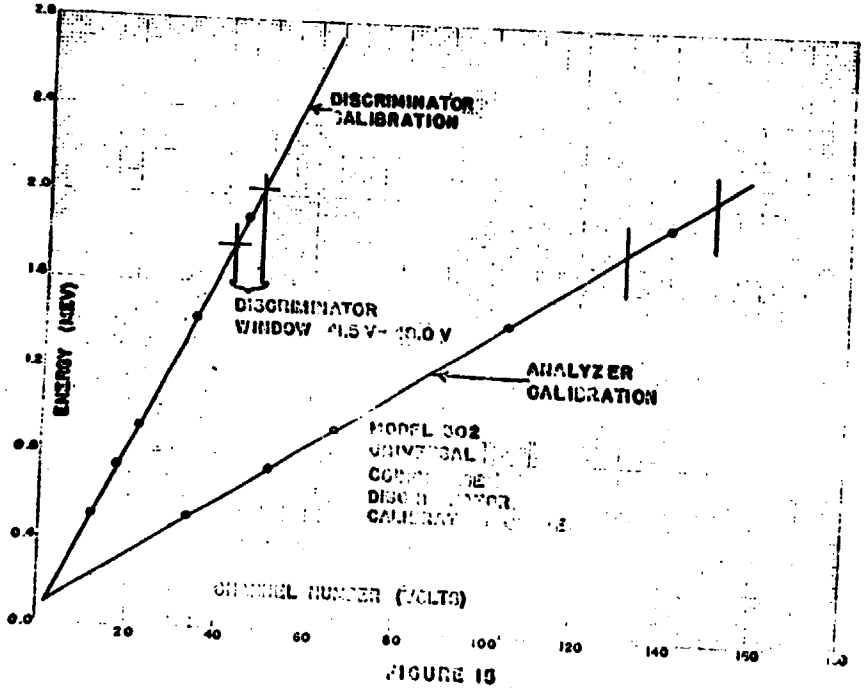
DISCRIMINATOR CALIBRATION
DISCRIMINATOR WINDOW
ANALYZER CALIBRATION
ENERGY (KEV)
MODEL 302
20
40
60
80
100
120
140
150

FIGURE 13

PROPOSED DECAY SCHEME FOR $Mn^{52m}$

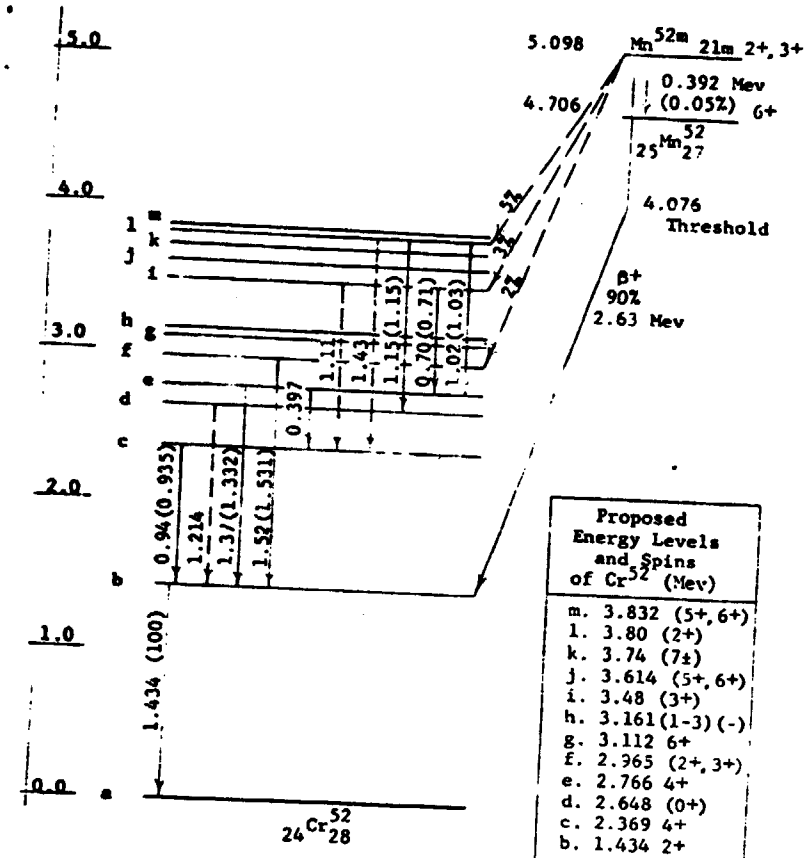


| Proposed Energy Levels and Spins of $Cr^{52}$ (Mev) |
|---|
| m. 3.832 (5+, 6+) |
| l. 3.80 (2+) |
| k. 3.74 (7±) |
| j. 3.614 (5+, 6+) |
| i. 3.48 (3+) |
| h. 3.161 (1-3) (-) |
| g. 3.112 6+ |
| f. 2.965 (2+, 3+) |
| e. 2.766 4+ |
| d. 2.648 (0+) |
| c. 2.369 4+ |
| b. 1.434 2+ |
| a. 0.0 0+ |

Figure 16

6 2

END